Tony McNally: Conceptualization, Funding acquisition, Methodology, Supervision, Writing- Reviewing and Editing. **Syeda Abbas**: Methodology, Investigation, Formal analysis, Data curation, Writing- Original draft preparation. **Nicole L. Kelly:** Methodology, Investigation, Formal analysis, Data Curation, Writing- Reviewing and Editing. **Georgios Patias**: Methodology, Investigation, Formal analysis, Data Curation, Writing- Reviewing and Editing**. John V. Hanna:** Methodology, Investigation, Formal analysis, Writing- Reviewing and Editing.

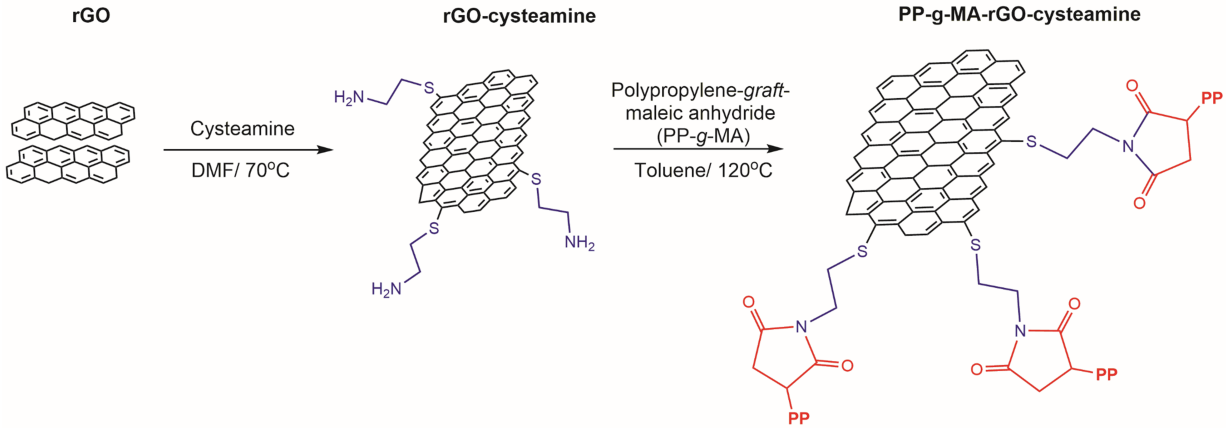
rGO
rGO-cysteamine
PP-g-MA-rGO-cysteamine
Cysteamine
DMF/ 70°C
Polypropylene-graft-maleic anhydride (PP-g-MA)
Toluene/ 120°C
H2N
S
NH2
O
N
PP

Cysteamine functionalised reduced graphene oxide modification of maleated poly(propylene)

Syeda S. Abbas[1], Nicole L.Kelly[2], Georgios Patias[3], John V. Hanna[2] and Tony McNally[1]*

[1]International Institute for Nanocomposite Manufacturing (IINM), WMG, University of Warwick, CV4 7AL, UK

Departments of [2]Physics and [3]Chemistry, University of Warwick, CV4 7AL, UK

*Corresponding Author. E-mail: t.mcnally@warwick.ac.uk (Tony McNally)

Telephone: 0044 (0)24 7657 3256

Abstract

Graphene oxide (GO) was reduced (rGO) and then functionalised with an amino terminated thiol molecule (cysteamine) *via* a thiol-ene click chemistry reaction to produce reduced graphene oxide-cysteamine (rGO-cyst). The presence of the C-S bond in the X-ray photoelectron spectrum (XPS) confirmed the reaction between the thiol in cysteamine and both the double bonds present on the rGO surface and the pyrazolic structures formed due to reduction. The rGO-cysyteamine was reacted with polypropylene-graft-maleic anhydride (PP-g-MA) to produce PP-g-MA-rGO-cysteamine, where the free amino group present on the rGO-cysteamine reacts with the maleic anhydride group of PP-g-MA. This was confirmed from solid state ^{13}C Magic-Angle-Spinning, Nuclear Magnetic Resonance (MAS NMR), Fourier transform infrared (FTIR) and XPS studies which demonstrated that a mixture of open and closed ring structures based on amides, imides and imines were formed. Growth of

the PP chain on the rGO surface was observed from electron microscopy imaging. Cysteamine acts like a 'cross-linker' between the rGO and PP-g-MA, increasing interfacial interaction between the two phases resulting in increased thermal stability and altering the crystallization behaviour of the maleated PP. The approach described could be used to compatabilise graphene oxide and a range of polymers to produce functional composite materials.

1. Introduction

The exceptional properties of the graphene family of materials continues to attract intense research interest and when combined with a large surface area (>2600 m^2 g^{-1})[1], can have a thermal conductivity up to ~5300 W m^{-1} K^{-1}[2], Young's modulus of 1 TPa [3-5], electrical conductivity in the order of 2 x 10^3 S cm^{-1})[6] and very high optical transparency (97.7%)[7]. The graphene single 2D layer of sp^2 hybridised carbon atoms are packed in a hexagonal structure[8] but are flexible enough to be wrapped or stacked into different 0D/1D/3D stuctures[9]. Few layer graphene, graphene/graphite nanoplatelets and graphene oxide also have useful properties, not as impressive as single layer graphene, but all can be used as a functional filler for polymers. The technical challenge is to translate these advantageous properties of graphene and its derivatives to polymers to produce functional composite materials. The translation of properties can only be achieved by uniform dispersion and distribution of the graphenic material throughout the polymer matrix and promoting the interfacial interactions between the components. However, due to high surface area of graphene(s), agglomerations can be formed within the polymer matrix. Therefore, to minimise agglomerations, graphene(s) must be modified with appropriate functional groups to promote compatability with the desired polymer[10, 11].

Recently, click chemistry has been successfully used for functiolalisation of graphene(s) due to the use of readily available reagents and ease of synthesis. Thiol-ene click reactions allows targeted addition to the C=C bond using a thiol reagent *via* heat (thermally) or light (photochemically)[12]. This then enables the desired functional group to be attached to the sp^2 carbons of the graphene[13]. Three different chemical routes were explored by Horacio J. Salavagione[14] to graft graphene with low molecular weight thiol-terminated poly(ethylene) (PE). For the copper catalysed azide-alkyne cycloaddition (CuAAC) route, the graphene must to be functionalised with an azide or an alkyne functional group, but Cu^I was utilised, which is toxic. For the thiol-yne reaction, an alkyne bond was required, which meant further functionalisation. Whereas, for the thiol-ene click reaction, it could directly react with the graphene, however, the reactivity of thiol groups decrease with increasing size of the thiol containing compound causing a low yield. In a recent study by Hu *et al*.[15], thiol-ene click chemistry was employed on different carbon nano-materials such as graphene, carbon nanotubes (CNTs) and fullerenes to functionalise with different groups, including –COOH, NH_2, NH_3Cl-$Si(OCH_3)_3$, alkyl and furyl groups. This was done *via* microwave radiation and used various thiol precursors such as cysteamine hydrochloride, L-cysteine hydrochloride, n-octadecyl mercaptan and cyseteamine. Yagci *et al.*[16] also modified fullerene with thiol functionalised polystyrene (PS-SH). Luong *et al.*[17] used cysteamine hydrochloride as the thiol precursor to functionalise graphene oxide *via* thiol-ene click chemistry using AIBN as the initiator. Using cysteamine as the thiol precursor proved advantageous as the thiol could be covalently bonded to the double bond of the graphene oxide and the amine at the terminal end was used for anchoring sites to adsorb nanoparticles. This precursor was also used in another study to functionalise fullerenes by Xu *et al.*[18]. Through this modification further functionalisation was allowed with biodegradable polymers. For this reason, cysteamine hydrochloride was used in this study to functionalise reduced graphene oxide. The thiol end

can react with the double bonds of the reduced graphene oxide and the free amino group is used to react with the maleic anhydride group of a polypropylene-graft-maleic anhydride (PP-g-MA). By doing so, the polymer would be covalently bonded to the reduced graphene oxide (rGO) *via* the thiol precursor. The PP chains of PP-g-MA are then available to co-crystallise when blended with PP.

Reaction between primary amine groups and the maleic anhydride group has been reported in many studies and is a fast process to make amic acid and/or imid bonds. Vazquez-Rodriquez *et al.*[19] studied the effects of different chain lengths of aliphatic diamines with PP-g-MA *via* an *in-situ* melt reaction. Through various techniques, amine and imide groups had been verified and diamines with low molecular weight had better adhesion between PP and poly(carbonate) (PC) when they were pressed together into two-layer films. In a more recent study[20], PP-g-MA was reacted with aniline, ($C_6H_5NH_2$) to make (PP-g-NHC_6H_5) which was used to compatibilize PP and carbon nanotubes. An increase in modulus was observed due to the π-π interactions between the C_6H_5 and the aromaticity of the CNTs. A similar finding was reported by Jin *et al*[21], who studied PP/CNT composites, using PP-g-MA as the compatibilizer and modified CNTs with diaminodecane, and Petrie *et al.*[22], who modified PP-g-MA with pyridine. As well as CNTs, graphene derivatives have also been functionalised with diamines[23], dianiline[24] and aminopropyltriethoxysilen (APTES)[25] for further reaction with PP-g-MA in an attempt to enhance compatibility with PP.

In this study, rGO was functionalised to make rGO-cysteamine (rGO-cyst). This was done *via* a thiol-click reaction using AIBN as a thermal initiator. Due to the low quantity of cysteamine used, it was characterised after the PP-g-MA was added and amine of the cysteamine reacted with the maleic anhydride to make PP-g-MA-rGOcyst. Furthermore, for comparison, rGO was also added to PP-g-MA without any cysteamine functionalization,

labelled PP-g-MA-rGO. This was done to aid characterisation and show how cysteamine functionalization of rGO allows compatibilisation with PP-g-MA *via* covalent bonding.

2. Experimental

2.1 Materials

Graphene oxide (GO) (1 nm thick/size of flakes 2-20 μm) was purchased from Abalonyx, polypropylene-graft-maleic anhydride (PP-g-MA) (average M_w ~9,100 by GPC and maleic anhydride 8-10 wt%), cysteamine hydrochloride (>97.0%) and 2,2'-Azobis (2-methylpropionitrile) (AIBN) (98%) were purchased from Sigma Aldrich. Sodium hydroxide pellets (>97%), dimethylformamide (DMF), methanol, ethanol, toluene and ammonia were obtained from Fisher, and hydrazine hydrate (78-82%) was purchased from Honeywell Fluka.

Synthesis of reduced graphene oxide (rGO)

GO was dispersed in water with a mixture of hydrazine hydrate and ammonia and heated at 90°C under reflux for 24 hours. This mixture was then filtered using vacuum filtration and washed with excess water, until the sample had neutral pH. The product was then dried in a vacuum oven at 60°C.

Synthesis of reduced graphene oxide-cysteamine (rGO-cyst)

The as prepared rGO was sonicated in an ultrasonic bath for 30 minutes in DMF. In the mean time a solution of AIBN and cysteamine was dissolved in DMF. After sonication, the rGO suspension was pre-purged with nitrogen. The AIBN cysteamine solution in DMF was then added to the rGO suspension and heated up to 70°C for 24 hours under nitrogen. The mixture was then cooled to room temperature (RT) and a solution of NaOH (1M) prepared in ethanol/water, which was then added to the rGO suspension and stirred. This mixture was

then filtered using vacuum filtration and washed with ethanol (2 times) and then with water (3 times). The product was dried in a vacuum oven at 60°C.

Grafting of polypropylene-graft-maleic anhydride with reduced graphene oxide-cysteamine (PP-g-MA-rGO-cyt)

PP-g-MA was dissolved in toluene at reflux temperature under N_2 to form a yellow solution. rGO-cyst was added to this solution (weight ratio calculated to be maleic anhydride: rGO-cyst 1:1) and stirred for 24 hours under N_2 at reflux temperature. This mixture was then washed with methanol repeatedly by hot filtration using a 0.2 μm polytetrafluoroethylene (PTFE) membrane. The product was dried in a vacuum oven at 80°C overnight to yield PP-g-MA-rGO-cyst.

2.2 Characterisation

All ^{13}C solid state MAS NMR measurements were performed at 9.4 T using a Bruker Avance 400 MHz spectrometer operating at ^{13}C Larmor frequency (ν_o) of 100.58 MHz. These experiments were performed using a Bruker 4 mm HX probe which enabled a MAS frequency of 12 KHz to be implemented. All ^{13}C data were acquired using single pulse/direct detection experiments using a $\pi/2$ nutation angle along with a relaxation delay between pulses of 30 s. During the data/FID acquisition period of these experiments strong ^{1}H decoupling (100 kHz in strength) was applied. The reported ^{13}C chemical shifts were externally referenced against the IUPAC recommended primary reference of Me_4Si (1 % in $CDCl_3$, δ_{iso} = 0.0 ppm), *via* the secondary solid alanine reference (δ_{iso} = 20.5 ppm) [26].

X-ray Photoelectron Spectroscopy (XPS) was carried out using a Kratos Axis Ultra DLD Spectrometer at RT and with a base pressure of 2 x 10^{-10} mbar, using a monochromated Al kα X-ray source. In order to prevent surface charging, the data was collected while the sample

was exposed to a flux of low energy electrons from the charge neutralizer built in to the hemispherical analyser entrance, with the binding energy scale retrospectively calibrated to the sp^3 C-C peak at 284.6 eV. The data was analyzed with the CasaXPS software package, using Shirley backgrounds and mixed Gaussian-Lorentzian (Voigt) line shapes and asymmetry parameters where appropriate. For compositional analysis, the analyser transmission function was determined using clean metallic foils to determine the detection efficiency across the full binding energy range.

Fourier-transform infrared (FTIR) spectra were recorded on a Bruker Tensor 27 Spectrometer equipped with an attenuated total reflectance (ATR) crystal and powder samples were measured with a scan range from 500 cm^{-1} to 4000 cm^{-1} with 4 cm^{-1} resolution.

Raman Spectra were recorded on a Renishaw inVia Reflex Raman Microscope with a 532 nm solid state laser and x5, x20, x50 objectectives. The laser (10 mW) was spot focused on the samples (powders made into pellets) with an exposure time of 2 mintues and a minimum of 5 collections

Scanning Electron Microscopy (SEM) micrographs were obtained using a Zeiss Sigma using InLens detector at 5kV. The samples imaged were sputter coated using an Au/Pd target. Transmission Electron Microscopy (TEM) micrographs were obtained using a Jeol 2100 TEM fitted with a Gatan Ultrascan 1000 camera. Samples for TEM analysis were prepared *via* drop-casting a few milliliters of sample dispersions after ultrasonication onto holey carbon grids, allowing the solvent to evaporate and leaving the sample to rest for 24 hours at RT.

X-ray Diffraction (XRD) measurements were completed on a Panalytical Empyrean instrument in Bragg-Brentano geometry with Co-K_α radiation (1.7903 Å) and a solid state Pixcel detector for fast data collection. A variable divergence slit was used to control the size

of the beam on the sample to be 6mm parallel to the beam and a beam mask of 15mm. 20 minute scans were collected in the range 4 – 40° 2θ with a step size of ~ 0.026 ° 2θ.

Differential Scanning Calorimetry (DSC) was performed using a Mettler Toledo (DSC1, model 700, 400W) and the data collected evaluated using a STARe Version 15.01 software package. The samples were measured between 25°C and 200°C at a heating and cooling rate of 10 K/min for two cycles. The thermograms were used to determine the melt temperature (T_m), crystallisation temperature (T_c), enthalpy of melting (ΔH_m), enthalpy of crystallisation (ΔH_c) and the percentage crystallinity (X_c) of PP. The crystallinity was calculated by dividing the ΔH_m or ΔH_c for the sample by the theoretical 100% crystalline value for PP, (ΔH_f: 209 J/g) [27].

Thermogravimetric Analysis (TGA) was carried out using a Mettler Toledo thermal analyzer in the temperature range 25°C to 800°C using a heating rate of 10 °K/min under nitrogen.

3. Results and Discussion

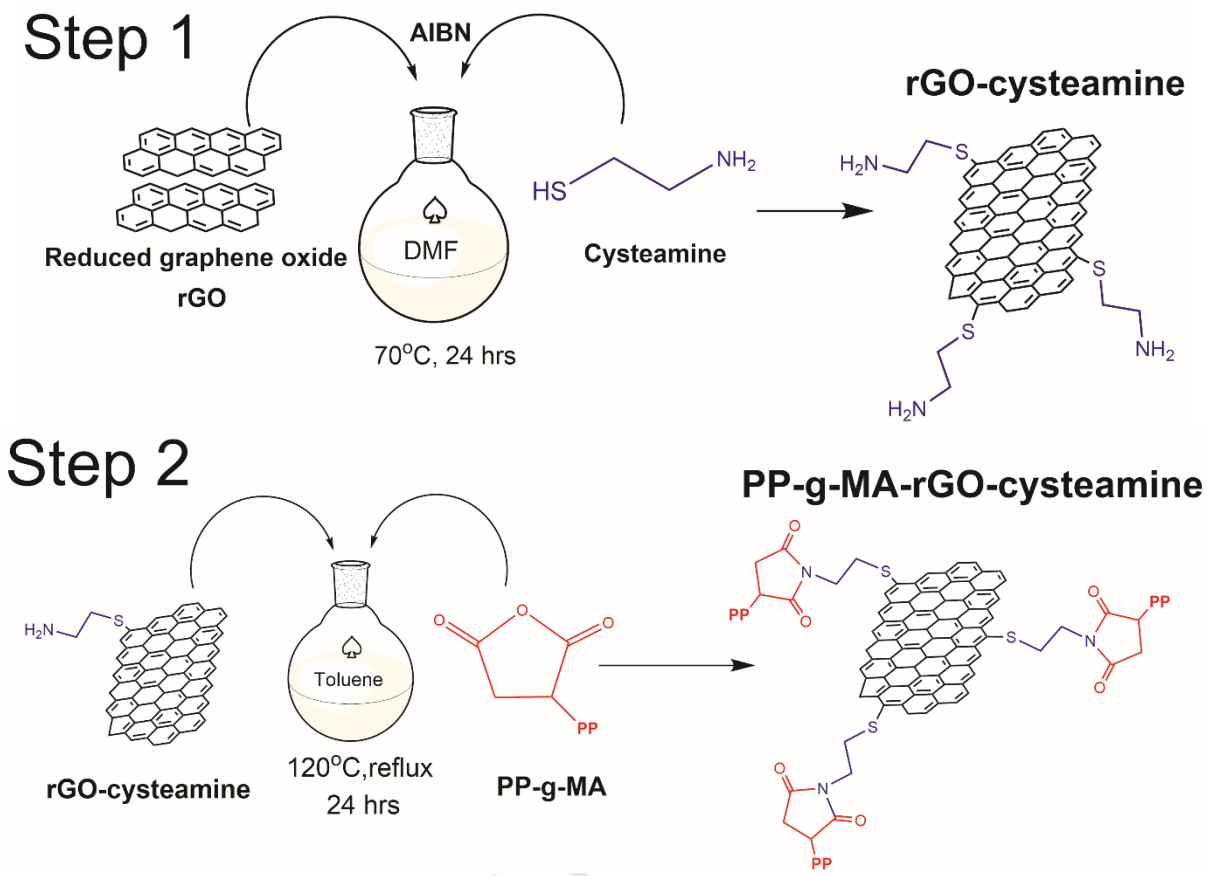

Figure 1. Step 1 illustrates the functionalisation of rGO with cysteamine to make rGO-cyst. Step 2 illustrates the solution blending process to mix rGO-cysteamine and PP-g-MA to make PP-g-MA-rGOcyst.

The cysteamine functionalisation of rGO (step 1) and reaction with PP-g-MA (step 2) is shown in Figure 1. In step 1, the reaction is thermally initiated by AIBN with the thiol-end of cysteamine reacting with the double bonds of the rGO. By doing so, the amine on the terminal end of the cysteamine is free to react in Step 2 (see Figure 1). Furthermore, cysteamine hydrochloride was used instead of cysteamine because the hydrochloride protected the free terminal amine group from reacting with any other functionalities on reduced graphene oxide. Although, the GO is reduced there are still some carbonyl functionalities present and to avoid a reaction between the carbonyls and the amine, cysteamine hydrochloride was used. However, after successfully making rGO-cyst, an excess

amount of base was added to remove the hydrochloride so that the amine is ready for the nucleophillic substitution reaction with the PP-g-MA [17].

In Step 2, the amino end of the cysteamine attached to the rGO reacts with the maleic anhydride group of the PP-g-MA to make a maleimide and give PP-g-MA-rGOcyst, thus enabling covalent attachment between the polymer, PP and the rGO *via* the cysteamine-maleic anhydride attachment. This happens in a two step condensation reaction. In the first step, PP-g-MA is dissolved in toluene in which it reacts with the primary amine to produce an open ring cycle, see Figure 2. The second step was carried out at an elevated temperature (120°C) and the intermediate process goes through a dehydration step for ring closure to yield N-substituted maleimide[28]. However due to high temperature and time, several by-products can also be formed, lowering the yield for the maleimide and therefore forming by-products, as illustrated in Figure 3. The secondary amide formed as the intermediate exists as a resonic structure. The lone pairs on nitrogen resonate between the nitrogen and carbonyl groups itself forming a cationic structure. This structure also equilibrates to form an imine as the carbonyl turns to a hydroxyl and an amide to a C=N. The presence of these resonic structures were verified using XPS and FTIR [29].

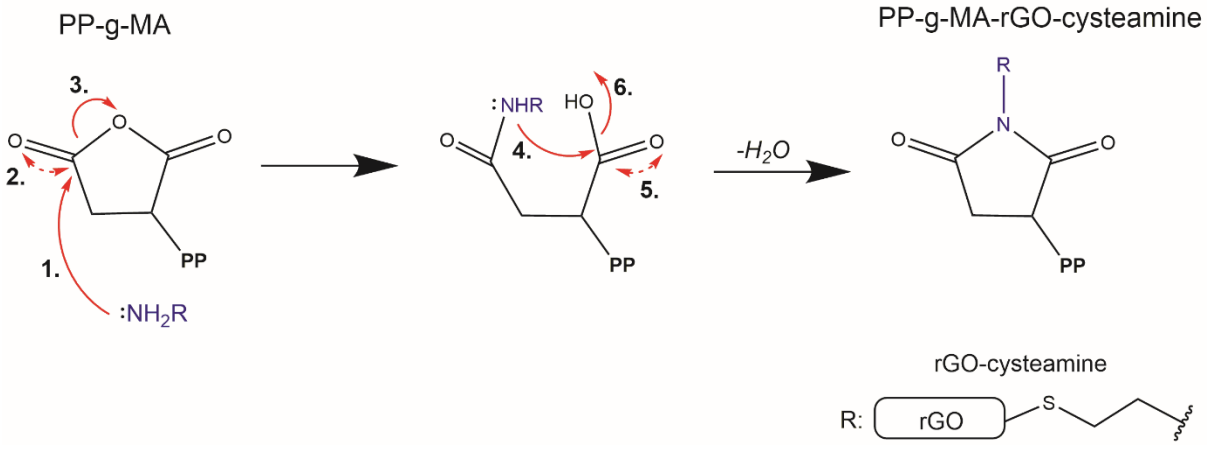

Figure 2. Two-step mechanism to synthesis PP-g-MA-rGOcyst.

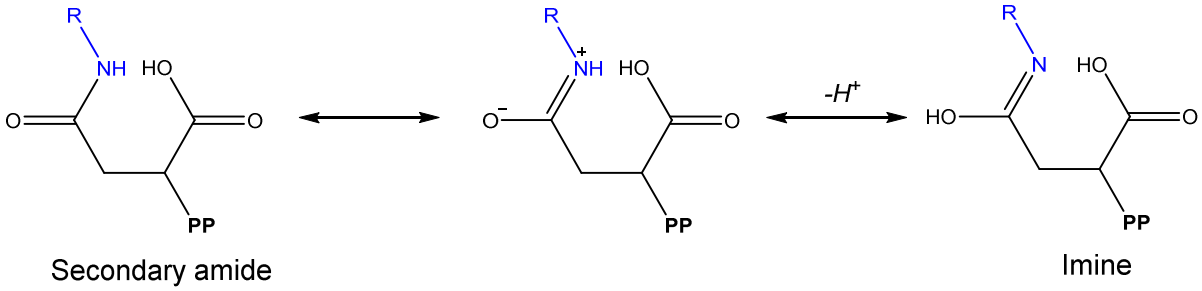

Figure 3. By-products formed *via* resonic structures.

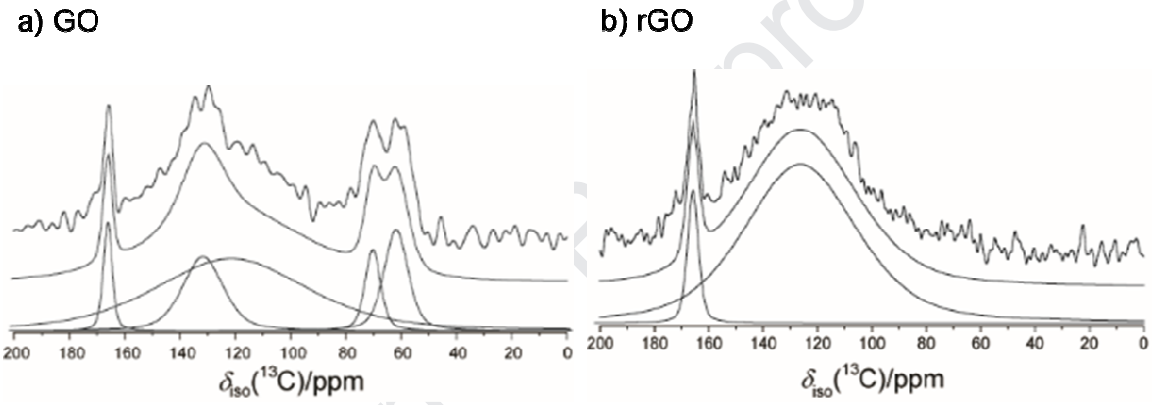

F igure 4. Solid state ^{13}C MAS NMR data from a) GO and b) rGO.

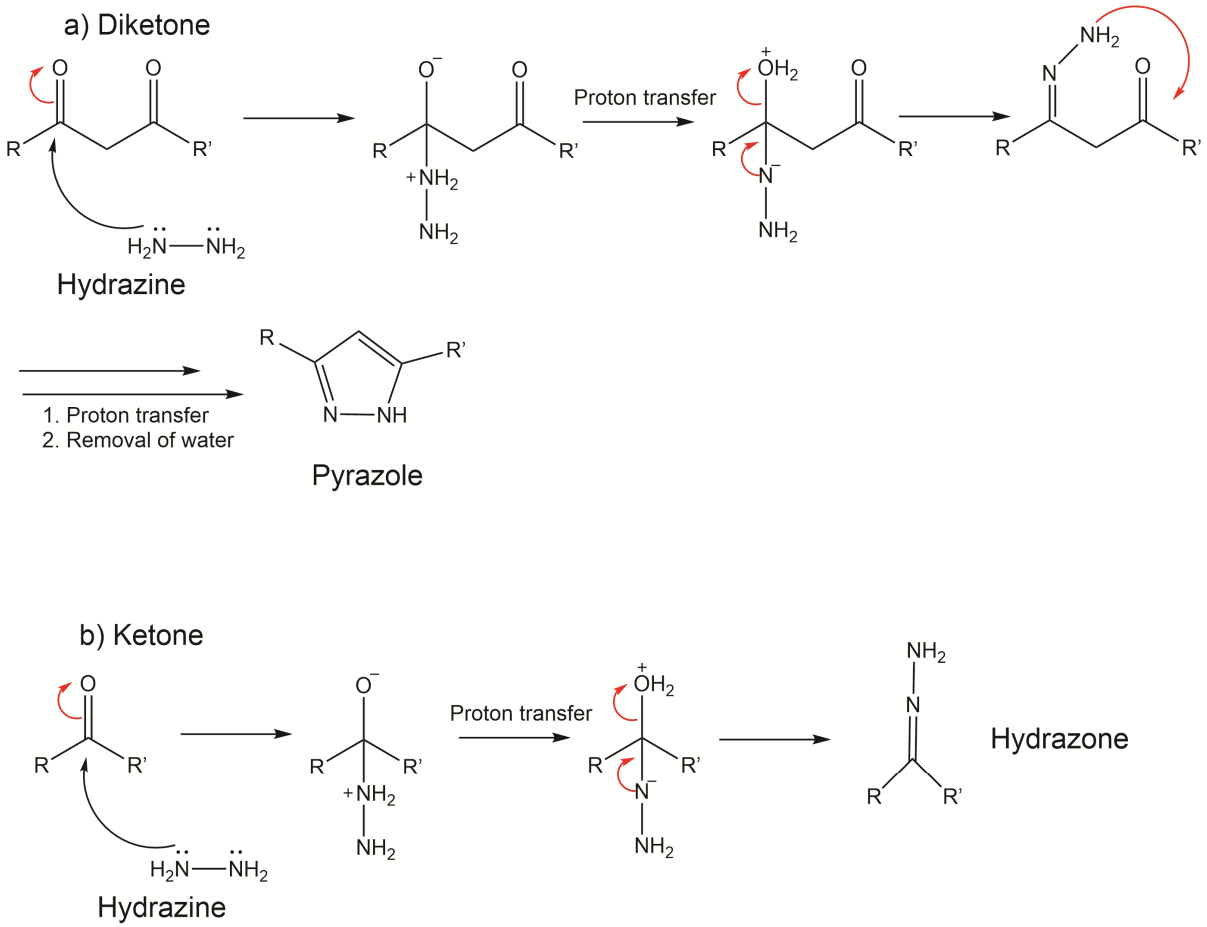

Figure 5. Mechanism for a) the formation of pyrazole by the attack of hydrazine with diketone and b) the formation of hydrazone by the attack of hydrazine with ketone[30, 31].

Before cysteamine functionalisation, GO was reduced using hydrazine hydrate and ammonia at 90°C in water. Use of hydrazine as a reducing agent is very common due to its ability to achieve a high degree of GO reduction without further reactions[32, 33]. Additionally, the presence of ammonia minimises aggregation of the rGO sheets produced[34]. Due to the presence of hydrazine, a large fraction of the oxygen containing functionalities on GO are removed, however, a small amount of N atoms are introduced. The ^{13}C MAS NMR of GO shows two carbonyl peaks for hydroxyl (-COH) and 1,2-epoxide functionalities at δ_{iso} = 68.45 ppm and δ_{iso} = 58.23 ppm, respectively, see Figure 4. There are two peaks corresponding to the bulk sp^2 hybridized graphene, one narrower resonance at δ_{iso} = 131.7 ppm and a broad

resonance at δ_{iso} = 121.4 ppm[35]. After reduction, the presence of the broader sp^2 peak in rGO at δ_{iso} = 126.3 ppm suggests that the sp^2 network was reformed by the hydrazine/ammonia treatment. Futhermore, the disappearance of the carbonyl peaks shows that the hydroxyl groups and the 1,2-epoxide groups located at the basal planes were completely removed by the reduction of hydrazine and the sp^2 networks reformed. However, a new peak emerged at δ_{iso} = 165.8 ppm for the rGO. This peak can be assigned to C=N bond formed in both pyrazole and/or hydrazine, from reaction of hydrazine with a ketone or an aldehyde[36, 37]. Formation of a five membered aromatic ring, pyrazole, with two adjacent nitrogen atoms can be formed if the hydrazine reacts with a diketone and shows ^{13}C MAS NMR signals between δ_{iso} = 150 ppm and δ_{iso} = 160 ppm[38] as seen in Figure 5a). Alternatively, hydrazine can also react with ketones to form a non-aromatic C=N to form hydrazone, as illustrated in Figure 5b). Either reactions take place due to the hydrazine acting as a nucleophile and reacting with the carbonyls on ketones, or diketones to form pyrazole or hydrazone giving rise to the peak at δ_{iso} = 163 ppm for C=N bond. This result has also been reported in other studies[30].

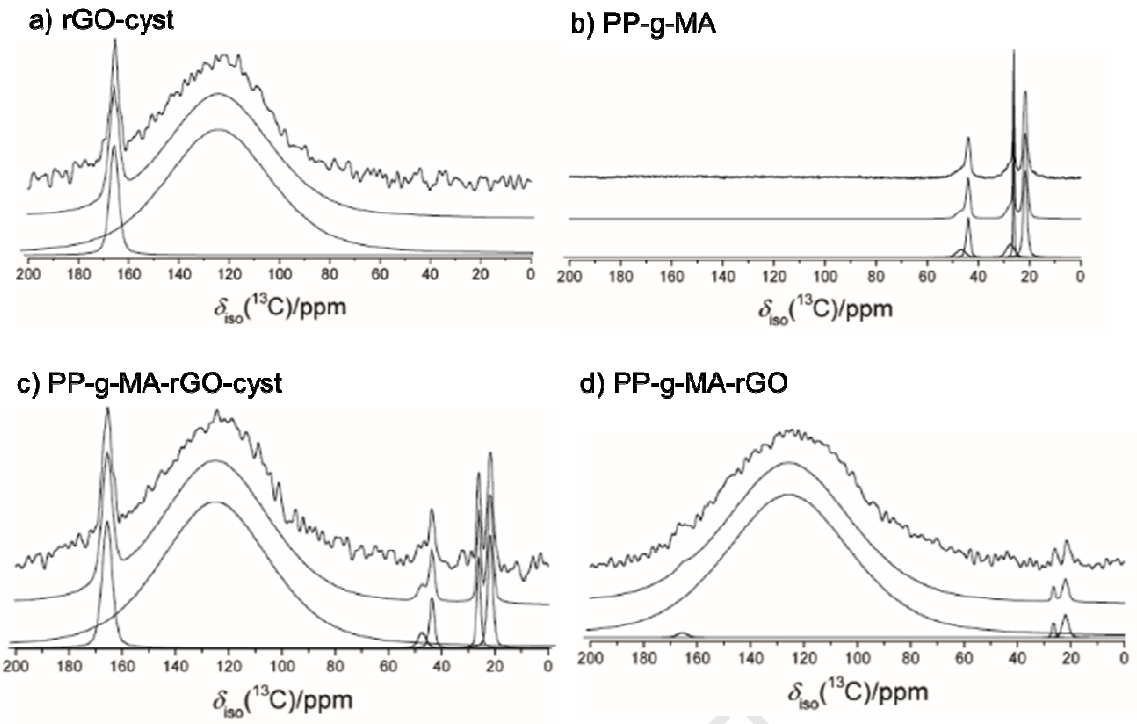

Figure 6. Solid state ^{13}C MAS NMR data from a) rGO-cyst, b) PP-g-MA, c) PP-g-MA-rGOcyst and d) PP-g-MA-rGO.

The solid state ^{13}C MAS NMR data for rGO-cyst, PP-g-MA, PP-g-MA-rGOcyst and PP-g-MA-rGO are shown in Figure 6. For neat PP-g-MA, the three intense resonances at δ_{iso} = 21.6 ppm, δ_{iso} = 26.1 ppm and δ_{iso} = 44.0 ppm are assigned to methylene, methine and methyl carbon species [39]. The CH and CH_2 group present in the maleic anhydride group of PP-g-MA exhibit partially resolved resonances at δ_{iso} = 46.8 ppm and δ_{iso} = 27.4 ppm, respectively[40]. For rGO-cyst, due to the low concentration of cysteamine added and the high abundance of rGO, any resonance associated with functionalisation would be masked in the MAS NMR spectrum. Therefore, no new resonances were observed in the ^{13}C MAS NMR spectra of rGO-cyst. To confirm bonding of cysteamine to rGO, ^{13}C MAS NMR data from PP-g-MA-rGOcyst was compared to that from PP-g-MA-rGO. If cysteamine wasn't grafted to rGO *via* the thiol bond, the amine wouldn't have reacted with the maleic anhydride group of the PP-g-MA; this is precisely what is observed from the ^{13}C MAS NMR data for

PP-g-MA-rGO in Figure 6). The sp^2 species is still present at δ_{iso} = 125.7 ppm and a less intense resonance at δ_{iso} = 26.5 ppm and δ_{iso} = 22.0 ppm can be observed for the methyl and methine carbons of the PP chain, respectively. However, the intensity of these resonances relative to the intensity of the resonances present in PP-g-MA-rGOcyst is insignificant. For PP-g-MA-rGOcyst system of Figure 6 c) there is a sp^2 resonance at δ_{iso} = 125.0 ppm, and four other resonances present at δ_{iso} = 21.8 ppm, δ_{iso} = 26.1 ppm, δ_{iso} = 43.6 ppm and δ_{iso} = 47.4 ppm corresponding to the methylene, methine and methyl of the PP chains, and the CH of the maleic anhydride group, respectively. This confirms the presence of cysteamine in the PP-g-MA-rGOcyst system, as there is a higher grafting of the polymer as seen from the difference in intensity in the 20-50 ppm region. Formation of an amide or maleimide due to the reaction between the amine in cysteamine with the maleic anhydride should exhibit a resonance at ~160 ppm, but due to the resonance observed at δ_{iso} = 165.6 ppm for pyrazole/hydrazone formation on the rGO surface this resonance must be unresolved with the existing peak (see Figure 6).

XPS measurements were performed to further validate the reduction of GO, synthesis of rGO-cyst and the grafting of PP-g-MA onto the rGO-cyst to make PP-g-MA-rGOcyst. From the survey spectra in Figure 7 a) and the results listed in Table 1, the reduction was successful as the O/% content decreased from 32.76% for GO to 9.80% for rGO. Additionally, the carbon-to-oxygen (C/O) atomic ratio increased for rGO relative to GO from 2.0 to 8.8 verifying the decrease in O content and that the reduction reaction was successful. Furthermore, a new peak evolved at ~399 eV for the nitrogen present on the rGO. As discussed in the ^{13}C MAS NMR section above, the presence of nitrogen is a result of the reaction between the carbonyls present at the basal edges of GO with hydrazine forming pyrazole and/or hydrazone structures on rGO edges. Furthermore, all graphene derivatives studied showed peaks for C1s and O1s, but one new peak evolved for PP-g-MArGO-cyst and

rGO-cyst at 163 eV for S2p. This is associated with the presence of cysteamine covalently attached to the rGO surface *via* thiol attachment and the polymer grafted *via* the free amine of the cysteamine.

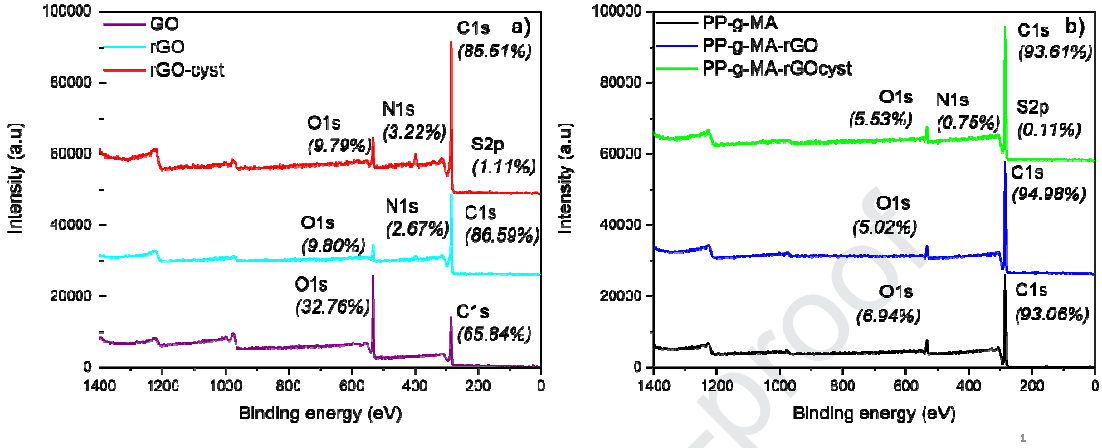

Figure 7. XPS survey for a) GO and rGO and b) rGO-cyst, PP-g-MA, PP-g-MA-rGO, and PP-g-MA-rGOcyst.

Table 1. XPS elemental composition of for GO, rGO, rGO-cyst, PP-g-MA, PP-g-MA-rGO and PP-g-MA-rGOcyst.

Sample name	**C /%**	**O /%**	**N /%**	**S /%**	**C/O**	**C/N**
GO	65.84	32.76	0	0.97	2.0	-
rGO	86.59	9.80	2.67	0.10	8.8	32.4
rGO-cyst	85.51	9.79	3.22	1.11	8.7	26.6
PP-g-MA	93.06	6.94	0	0	13.4	-
PP-g-MA-rGO	94.98	5.02	0	0	18.9	-
PP-g-MA-rGOcyst	93.61	5.53	0.75	0.11	16.9	128.8

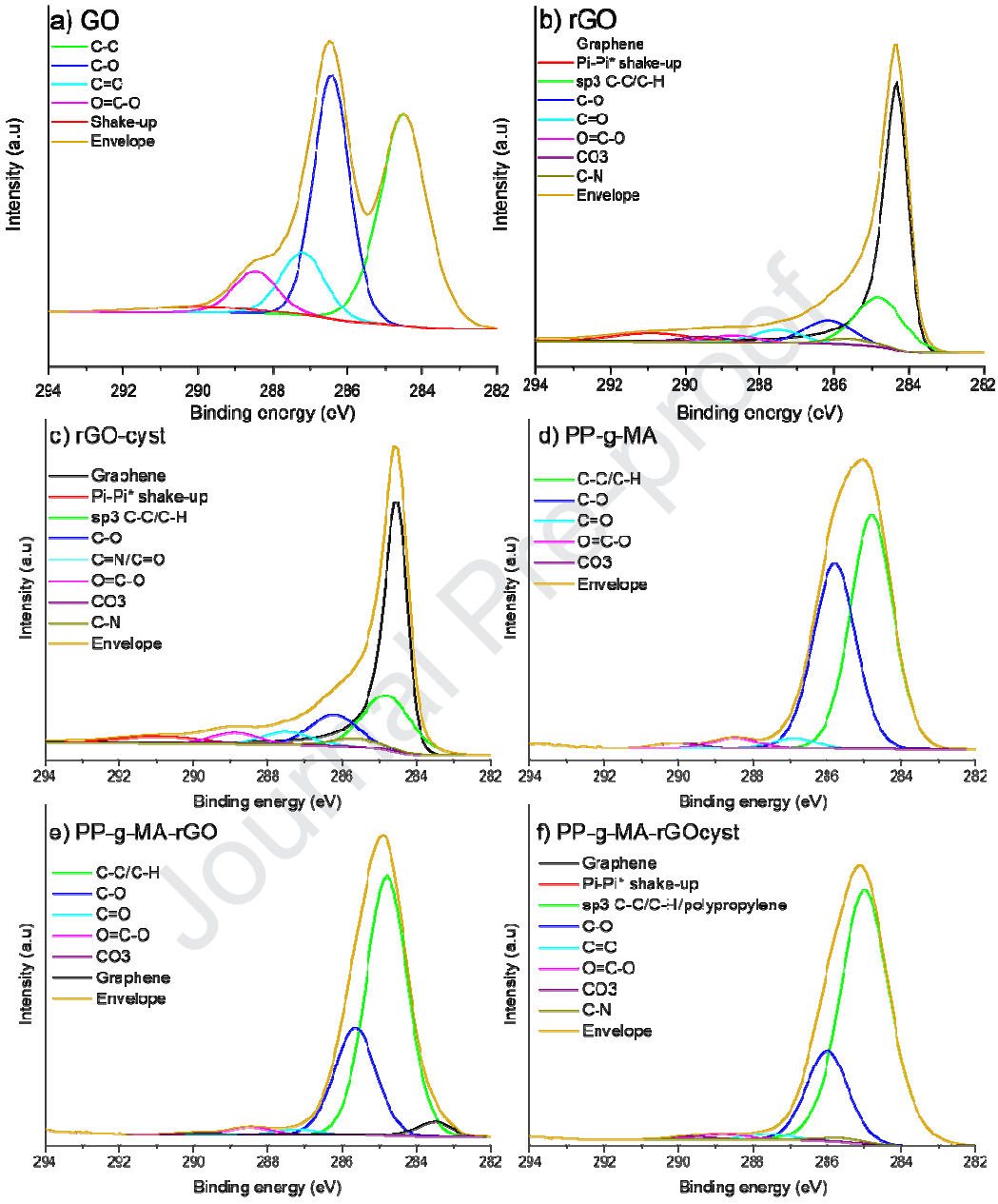

Figure 8. C1s spectra for a): GO, b): rGO, c): rGO-cyst, d): PP-g-MA, e): PP-g-MA-rGO and f): PP-g-MA-rGOcyst.

Due to the successful reduction of rGO, most of the oxygen related functional groups were removed so only a small amount of carbonyl peaks are present, see the C1s spectra for rGO-

cyst in Figure , showing binding energies for C-C/C-H (284.8 eV), C-O (286.15 eV), C=O (287.5 eV), O=C-O (288.7 eV) and sp^2 C shake up (291.13 eV). In the C1s spectra of PP-g-MA, the two main peaks were for C-C/C-H and C-O due to the PP chain and maleic anhydride group present, respectively. The same peaks are seen for PP-g-MA-rGO in the C1s spectra, as well as additional peaks for the rGO present. For PP-g-MA-rGOcyst and rGO-cyst, a new peak emerged in the C1s spectra for the C-N bond of the cysteamine group at 285.6 eV which wasn't present in rGO. The presence of this peak confirms the presence of cysteamine on rGO. Furthermore, for PP-g-MA-rGOcyst, the C-C (285 eV) and C-O (286 eV) bonds significantly increase due to the PP chain and the maleic anhydride groups present relative to rGO-cyst.

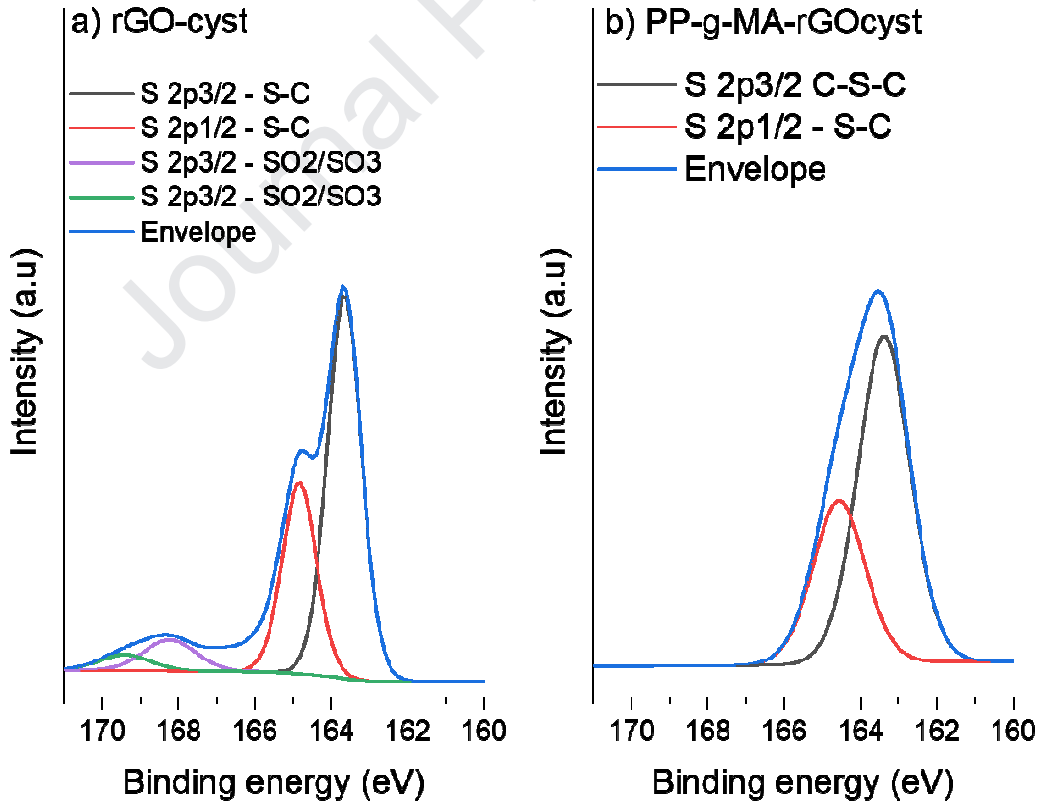

Figure 9. S2p spectra for a): rGO-cyst and b): PP-g-MA-rGOcyst.

Table 2. Deconvulated XPS data for S2p for rGO-cyst and PP-g-MA-rGOcyst.

Sample name	Binding energy /eV	Atomic /%	Bonding environment
rGO-cyst	163.65	41.01	S 2p3/2-S-C
	164.83	40.15	S 2p1/2- S-C
PP-g-MA-rGOcyst	163.38	50.53	S 2p1/2-S-C
	164.56	49.47	

Due to the binding energy of C-S overlapping with the binding energy of C-C (sp^3), it is not possible from the C1s spectra to accurately determine the presence of low atomic percentage S moieties present in rGO-cyst. Therefore, the S2p spectrum is used for further validation of the formation of the C-S bond, see Figure and Table 2. For rGO-cyst, in the S2p spectrum, two main peaks were observed at 163.65 eV and 164.83 eV assigned to the $2p_{3/2}$ of C-S-C and $2p_{1/2}$ S-C bond, respectively. The evolution of these two new peaks verify covalent attachment between cysteamine and the double bonds present on the rGO *via* the thiol. These peaks are also present in the S2p spectrum for PP-g-MA-rGOcyst, again confirming the cysteamine functionalised rGO attached to the PP-g-MA. In contrast, the PP-g-MA-rGO spectrum showed there was no sulphur or nitrogen present and, therefore no covalent attachment between the rGO and the PP-g-MA, see also Table 1.

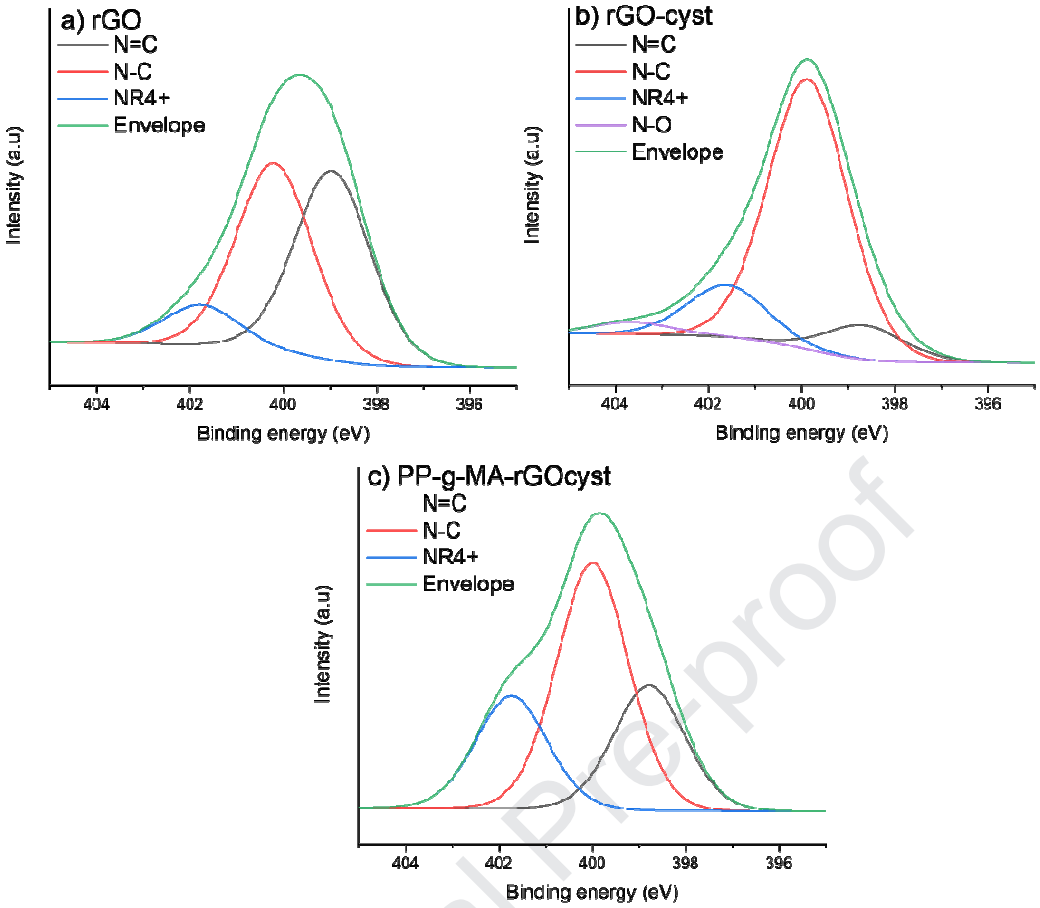

Figure 10. N1s spectra for a) rGO, b) rGO-cyst and c) PP-g-MA-rGOcyst.

Table 3. Deconvulated data for N1s of rGO, rGO-cyst and PP-g-MA-rGOcyst.

Sample name	Binding Energy /eV	Atomic/ %	Bonding environment
rGO	398.95	45.42	N=C
	400.19	45.16	N-C
	401.77	9.42	$(NR_4)+$
rGO-cyst	398.65	9.2	N=C
	399.86	73.57	N-C
	401.6	14.11	$(NR_4)+$

	403.65	3.12	N-O
	398.78	25.75	N=C
PP-g-MA-rGOcyst	399.99	50.96	N-C
	401.73	23.29	$(NR_4)+$

For rGO, three main peaks were seen in the N1s spectra at 398.65 eV, 399.86 eV and 401.6 eV for N=C, N-C and NR_4^+, respectively. This suggests that pyrazoles were formed at the basal plane of rGO surface as there are equal amounts of N=C (45.42 %) and N-C (45.16 %) bonds. However, when cysteamine is added to rGO, the ratio of these bonds changes from 45.42% (N=C) and 45.16 % (N-C) to 9.2 % (N=C) and 73.57 % (N-C), respectively. This is due to the addition of a primary amine, increasing the C-N bond [41]. Furthermore, the thiol end of cysteamine, can also react with the C=N bond in pyrazole to form a single C-N bond, thereby increasing the amount of C-N bonding and decreasing the C=N bonding[42]. Whereas when reacted with PP-g-MA, the 9.2% of N=C changed to 25.75% at 398.78 eV and N-C changed from 73.57% to 50.96% at 399.99 eV. These results show that most of the primary amine of the cysteamine group of rGO-cyst, reacted with the maleic anhydride group to form imine (C=N) and imide (N-C) bonds which results in a mixture of open and closed ring structures, as seen in Figure 3 above. The binding energy at 401.73 eV corresponds to the cationic structure as a resonic structure in Figure 3, at 23.29%. The N1s XPS data for PP-g-MA-rGOcyst shows that there were a mixture of both open and closed ring structures due to the amine reacting with the maleic anhydride group.

The FTIR spectrum of GO shown in Figure 1 a) shows a broad band associated with the hydroxyl groups present between 2877 cm^{-1} and 3678 cm^{-1} and carbonyl and epoxide

peaks at 1720 cm^{-1} and 1620 cm^{-1}, respectively [35]. After reduction to rGO, no hydroxyl peaks can be seen and most of the carbonyls and epoxide peaks are supressed due to successful reduction by the hydrazine treatment. Even though the majority of rGO consists of C=C bonds, the $\nu_{C=C}$ signal is very weak, due to the symmetrical environment of these bonds causing only a small change in the dipole moment [42]. For rGO-cyst, new peaks evolve at 1554 cm^{-1}, 1439 cm^{-1} and ~864 cm^{-1} that were not present for rGO, corresponding to the stretching vibrations of amine and C-S vibrations. Sulphur containing moieties usually absorp at low frequencies in the infrared region of the spectrum[33]. The peaks present for amine and C-S bonds in FTIR spectrum confirm the presence of cysteamine grafted to rGO *via* the thiol[43].

For PP-g-MA, the characteristic FTIR peaks can be seen at 2952 cm^{-1} for symmetrical –CH stretching from the methyl groups of the PP chain, Figure 11 b). Whereas, the peaks at 2914 cm^{-1}, 1458 cm^{-1} and 1377 cm^{-1} are attributed to the asymmetrical –CH stretching, asymmetrical and symmetrical bending modes from the methyl –CH bonds, respectively. The peak at 1300 cm^{-1}, is derived from various bending modes of the methylene group (scissoring, rocking, wagging and twisting)[44]. The FTIR spectrum of PP-g-MA also shows peaks at 1780 cm^{-1} and 1710 cm^{-1} that are attributed to the carbonyls of the maleic anhydride groups. These peaks are significantly reduced in intensity when grafted to rGO-cyst and the broad peak at 1568 cm^{-1} confirms the presence and formation of the amide linkages between PP-g-MA and rGO-cyst. Formation of an amide from maleic anhydride and primary amine is a fast reaction however, imide formation requires the removal of water and is a much slower reaction that needs high temperature to proceed [19]. The two peaks at 1710 cm^{-1} and 1780 cm^{-1} for the carbonyls present result in overlap of the absorption peaks of amide and imide bonds but zooming in on this region of the spectrum (see circled region in Figure 11 b), another peak can be observed at 1743.63 cm^{-1}, attributed to the imide bond [45].

From the FTIR, it can be seen that mixtures of amides and imides were formed, in agreement with the XPS measurements. The reaction itself did not go to completion and formed mixtures of amides, imides and imines. To confirm this, the interfacial melt reaction is estimated by comparing the relative intensity of the imide C=O stretching band (I_{1739}) and amide N-H bending (I_{1566}) with respect to a band in the fingerprint region (I_{1110}, C-C stretching), which does not change for both PP-g-MA-rGO and PP-g-MA-rGOcyst. From the values listed in Table 4, there is an apparent increase in the amide and imide bonds in PP-g-MA-rGOcyst relative to PP-g-MA-rGO. Due to the presence of rGO-cysteamine in PP-g-MA-rGOcyst a higher degree of melt-interfacial interaction is observed due to the higher concentration of amines present to react with the anhydride groups associated with PP-g-MA. The presence of amide and imide bonds in PP-g-MA-rGO is due to small quantity of pyrazoles still present on the rGO surface reacting with PP-g-MA.

Furthermore, similar peaks can be seen for PP-g-MA-rGO, but this is associated with the low concentration of pyrazoles still present on the rGO surface. Furthermore, doublets were present for PP-g-MA at 2952 cm^{-1} and 2914 cm^{-1} assigned to C=C and C-H stretching in the PP chains, which was also present for the PP-g-MA-rGOcyst. This also further validates the grafting of PP-g-MA-rGOcyst [23, 24].

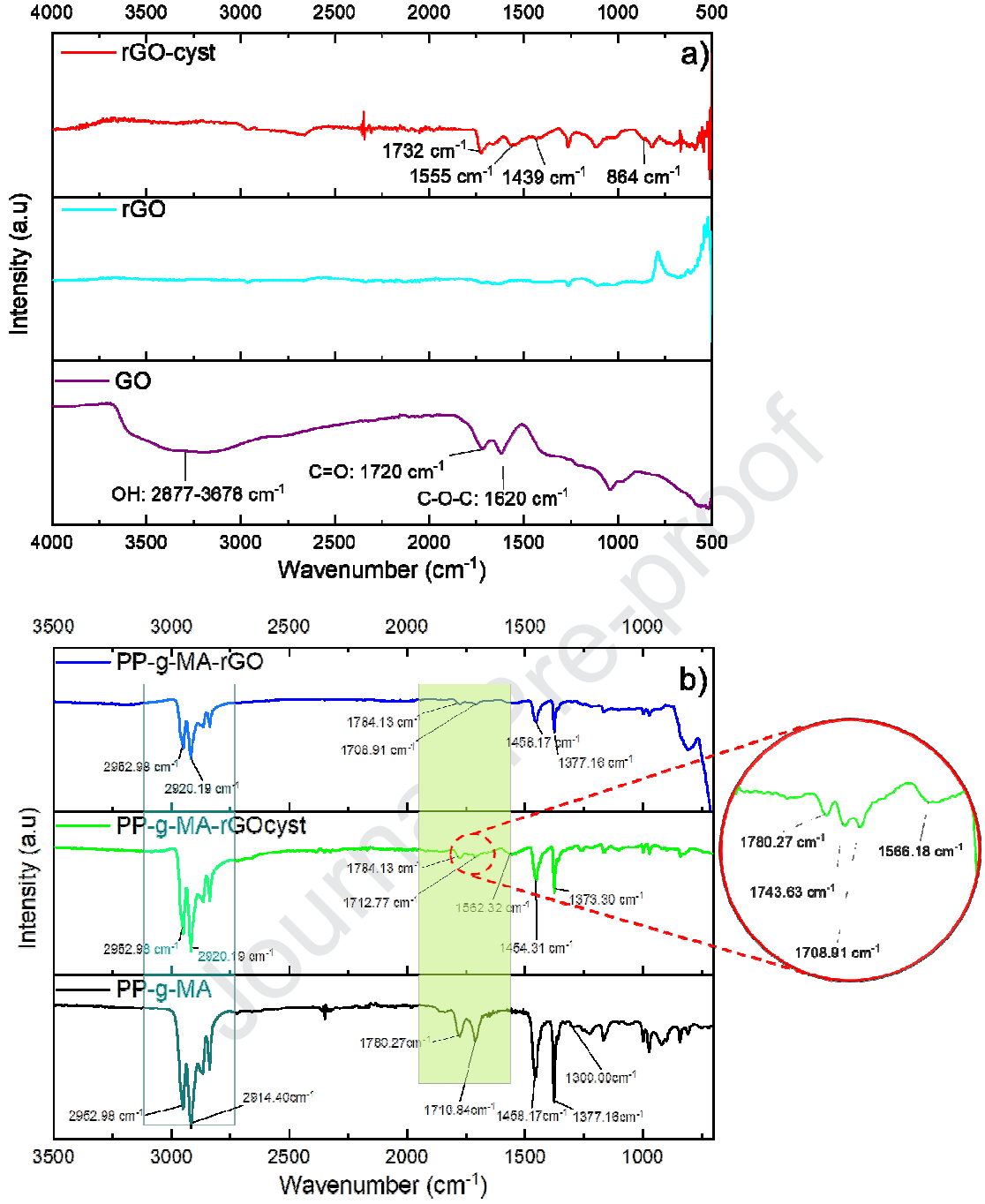

Figure 11. FTIR spectra for a) GO, rGO and rGO-cyst and b) PP-g-MA-rGO, PP-g-MA-rGOcyst and PP-g-MA. Inset in the red circle shows the expanded region between 1500-1800 cm^{-1}.

Table 4. Ratio of the intensity of the imide/amide peak to the peak at 1110 cm^{-1} for PP-g-MA-rGO and PP-g-MA-rGOcyst.

	PP-g-MA-rGO	PP-g-MA-rGOcyst
Imide (I_{1739}/I_{1110})	0.61	11.86
Amide (I_{1543}/I_{1110})	0.59	6.17

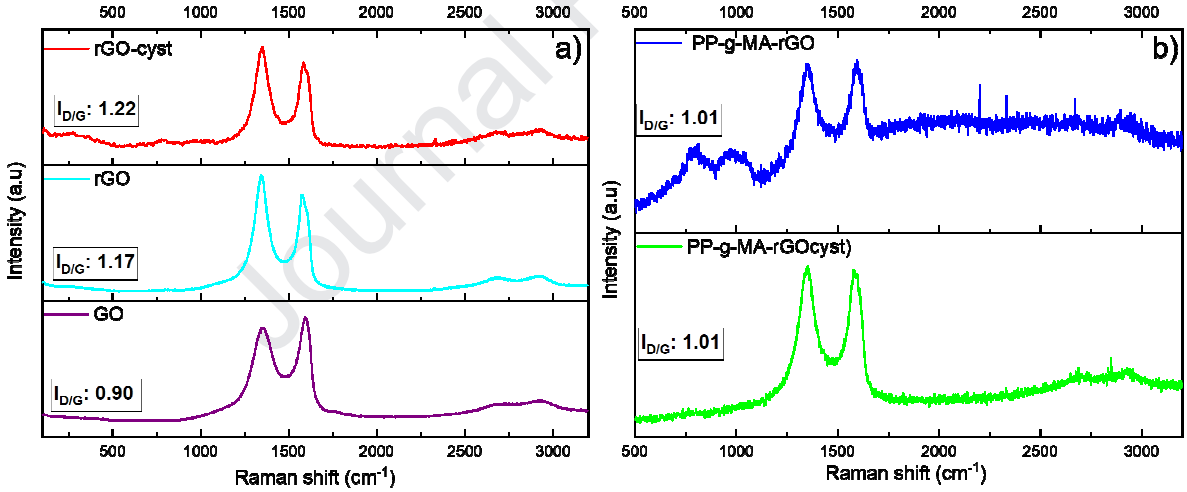

Figure 12. Raman spectra of a) GO, rGO, rGO-cyst, and b) PP-g-MA-rGO and PP-g-MA-rGOcyst.

Table 5. D and G band wavenumbers and the intensity ratio, $I_{D/G}$ for GO, rGO, rGO-cyst, PP-g-MA-rGOcyst and PP-g-MA-rGO.

Sample name	D band (cm^{-1})	G band (cm^{-1})	$I_{D/G}$
GO	1345	1595	0.91
rGO	1339	1582	1.17
rGO-cyst	1349	1589	1.22
PP-g-MA-rGOcyst	1349	1582	1.01
PP-g-MA-rGO	1345	1582	1.01

Figure 12 shows the Raman spectra for rGO, rGO-cyst, PP-g-MA-rGOcyst and PP-g-MA-rGO and the two characteristic peaks at ~1340 cm^{-1} and ~1580 cm^{-1} are assigned to the D and G bands, see values listed in Table 5. The D band correlates to the defects and the disorder present in the graphitic structure, whereas the G band is related to the in-plane bond-stretching motion of sp^2 carbon to sp^3 hybridized carbon caused by the destruction of the sp^2 structure of graphite by covalent grafting[46-48]. The ratio between the intensity of the D to G bands ($I_{D/G}$) is a measure of the degree of defects on the GO surface caused by covalent attachment of functional groups. When GO was reduced to rGO the G band shifted from 1595 cm^{-1} to 1582 cm^{-1}, similar to that reported in the literature for GNPs [35], confirming the sp^2 network was restored. A slight increase in the G band for the rGO-cyst was obtained relative to that for rGO. The change in G band is derived from the dopants grafted onto the

GO, electron donors shifting the G band to lower frequency and electron acceptors shifting the G band to higher frequency[49]. For example, in a previous study [50], GO was grafted with long chain alkylamine which induced a positive inductive effect on the amine group attached to the GO therefore downshifting the G band relative to that for non-grafted GO. In this current study cysteamine was used which has a thiol and an amine attached at either end of the molecule, causing an inductive effect on both ends. This results in an increase in the G band relative to that for rGO. Furthermore, $I_{D/G}$ increases from 0.91 to 1.17 on reduction of GO to rGO showing an increase in defect density on the surface of rGO due to the removal of oxygen functional groups and the introduction of pyrazolic groups on the basal planes of rGO [51]. $I_{D/G}$ increased further when functionalised with cysteamine to 1.22, showing a higher degree of disorder on the rGO sheets due to the anchoring of cysteamine on the rGO surface. However, for the PP-g-MA-rGOcyst $I_{D/G}$ decreasd to 1.01 relative to rGO and rGO-cyst. For rGO and rGO-cyst, the carbon double bonds are breaking on the surface of rGO to form new covalent bonds which is causing the disorder. Whereas, for PP-g-MA-rGOcyst, the maleic anhydride is reacting with the amino groups of the cysteamine attached rather than directly reacting with the surface of rGO. Thus, causing no further defects or disorder on the surface of rGO and showing a lower shift for the D band and lower $I_{D/G}$ [52].

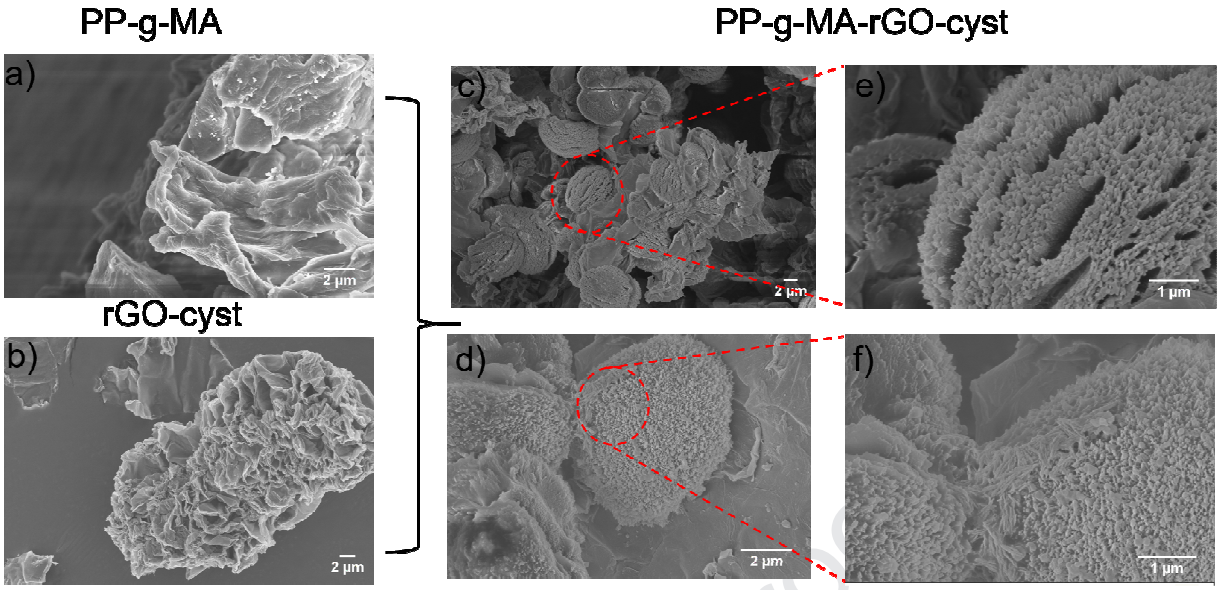

Figure 13. SEM images of a) PP-g-MA, b) rGO-cyst, c)-d) PP-g-MA-rGOcyst. (area in red circles expanded and shown in e) and f))

The morphology of the samples was examined using SEM imaging and the images obtained for PP-g-MA and rGO-cyst compared with those of solution blended PP-g-MA-rGOcyst, Figure . The functionalisation of rGO with cysteamine resulted in a coating of the rGO layers, Figure b). When rGO-cyst was solution blended with PP-g-MA, Figure c), spherical like layers of polymer growth formed on the rGO-cyst layers. Magnification of this spherical polymer growth is shown in Figure e), where it appears the rGO-cyst layers provided a surface for the polymer to grow from due to the covalent attachment of the maleic anhydride groups with the cysteamine. The PP-g-MA polymerizes on the edges of the rGO-cyst and aids exfoliation of the layers, see Figure c) and 13 f).

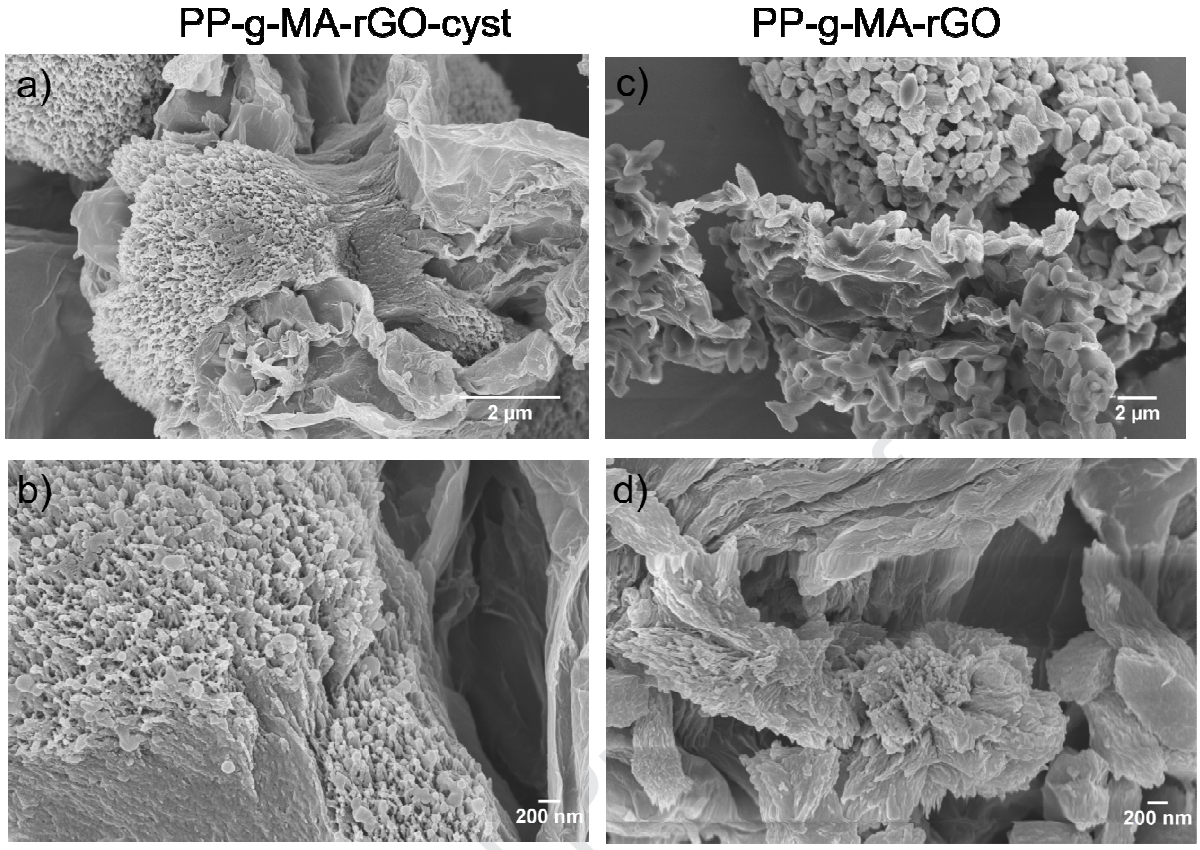

Figure 14. SEM images of a)-b) PP-g-MA-rGOcyst and c)-d) PP-g-MA-rGO.

Figure shows SEM images comparing PP-g-MA-rGOcyst and PP-g-MA-rGO. Both have polymer coating on the surface of rGO. However, for PP-g-MA-rGOcyst, the polymer seems to be attached to the rGO surface and is growing from it. Whereas for PP-g-MA-rGO, the surface of rGO is covered with 'rod-like' polymer, Figure 14 c). From these images it can be seen that the coating of PP-g-MA on neat rGO is scattered and only present on the surface but the growth of PP-g-MA on rGO-cyst is more uniform and on the edges of rGO-cyst forming spherical growth patterns and exfoliating the layers of rGO-cyst. The difference in the coating of the polymer on each shows that covalent bonding between the PP-g-MA and rGO-cyst plays a vital role in the dispersion of the nanofiller within the polymer matrix.

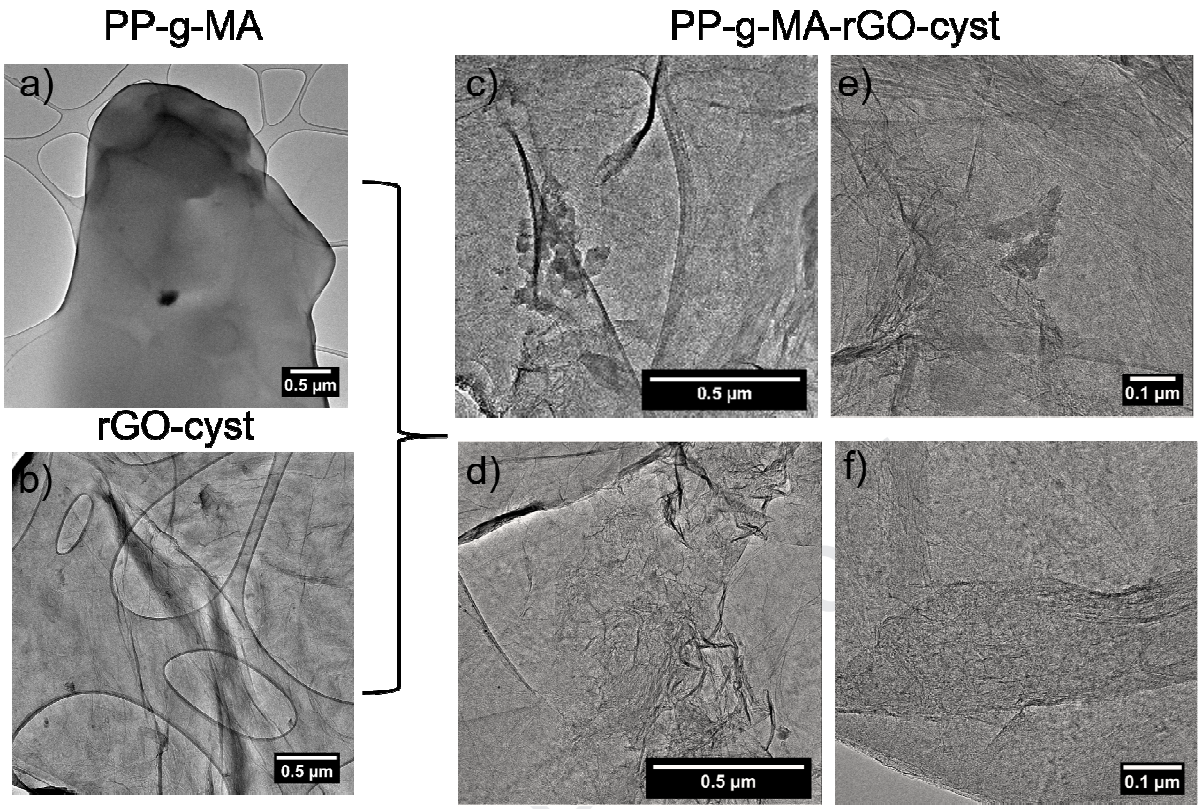

Figure 15. TEM images of a) PP-g-MA, b) rGO-cyst, c)-f) PP-g-MA-rGOcyst.

This observation is further verified by TEM imaging as seen in Figure 15. The TEM image of rGO-cyst ((Figure 15 b)) shows a wrinkled and folded surface suggesting functionalisation causes the layers to fold. The TEM image for PP-g-MA-rGOcyst shows even more wrinkles and folds within layers. Figure 15 c) shows that within these wrinkles and folds are clusters of spherical polymer particules, as seen in the SEM images. As the PP-g-MA crystallizes and entangles on the rGO-cyst surface, the surface puckers and therefore alters the rGO-cyst morphology[25]. Furthermore, from the TEM it is clear the high level of rGO-cyst dispersion in the PP-g-MA (Figure 15e) - 15 f)).

The XRD curves for GO, rGO and rGO-cyst are shown in Figure 16 a). For GO, a sharp peak at $2\theta = 12.20°$ corresponds to an interlayer spacing of 0.84 nm, a value greater than that normally reported for graphite (0.38 nm) due to the presence of the oxygen

functional groups between layers, increasing the interlayer spacing. After the reduction process, this sharp peak disappears and a broad peak at 2θ = 28.25° evolves, associated with the (002) basal plane which has an interlayer spacing of 0.37 nm close to that again for graphite. This is futher evidence for successful reduction of GO. Furthermore, the appearance of this new peak and the disappearance of the peak at ~12° shows that the rGO layers re-stack due to van der Waals forces and the conjugated network is restored by eliminating the oxygen-containing groups. Additionally, rGO also has a shoulder peak at 2θ = 25.15° derived from the bimodal or multimodal nature of the interlayer spacing of rGO. For rGO-cyst, any increase in the interlayer spacing caused by functionalisation with cysteamine cannot be determined as the corresponding peaks overlap.

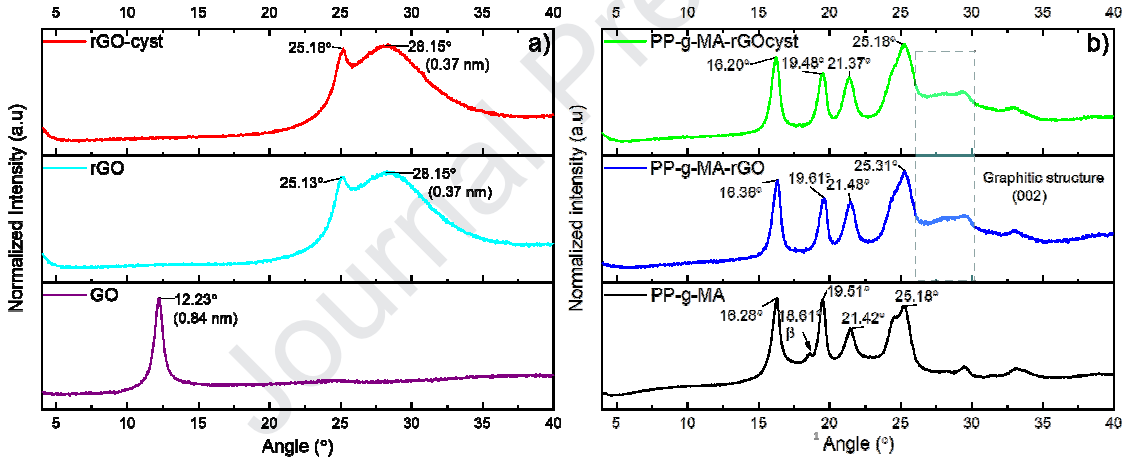

Figure 16. XRD curves for a) GO, rGO and rGO-cyst and b) PP-g-MA-rGOcyst, PP-g-MA-rGO and PP-g-MA.

After cysteamine functionalisation of rGO, the peak associated with the (002) basal planes for the graphitic structure broadened to between ~25 and 32° which can be attributed to the random order of the stacking of the rGO sheets [52]. This broad peak was also seen for the two composite materials, PP-g-MA-rGO and PP-g-MA-rGOcyst confirming the presence of rGO within the composite. Furthermore, PP-g-MA-rGOcyst shows additional

characteristic peaks at 2θ = 16.20°, 19.53°, 21.37° and 25.18° corresponding to the (110), (040), (130), (111) and (131) + (041) crystalline planes for the α-form of PP, similar to PP-g-MA-rGO[53]. Whereas for neat PP-g-MA, there was an extra peak at 2θ= 18.46° for the (300) plane of the β crystal [54]. This peak was absent for the composites, perhaps due to the increased amorphous phase caused by the presence of rGO and overlapping of the associated peaks.

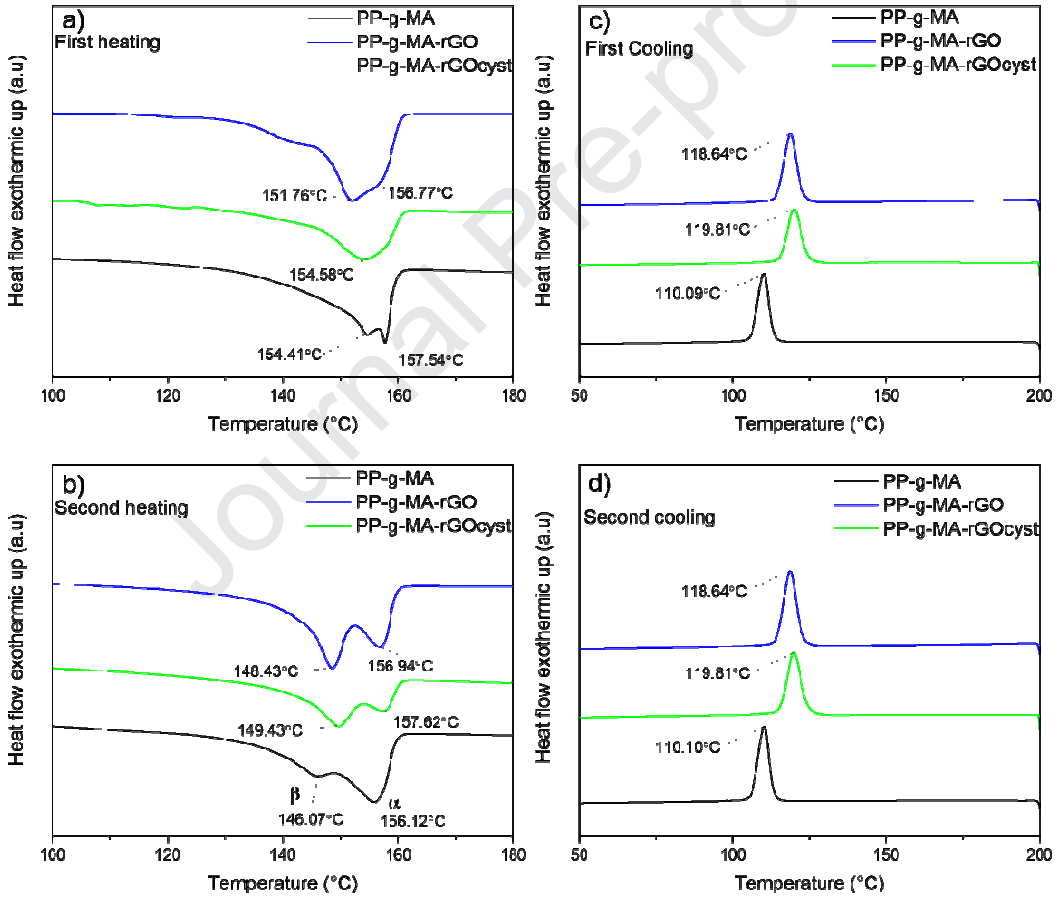

Figure 17. DSC curves of a) melting and b) crystallization of neat PP-g-MA, PP-g-MA-rGOcyst and PP-g-MA-rGO.

Table 6. Values for melting transition enthalpies (ΔH_m/ J g^{-1}), crystallization transition enthalpy (ΔH_c/ J g^{-1}), melting temperature(T_m/ °C), crystallization temperature (T_c/ °C) and crystalline content for (X_c/%) of PP-g-MA, PP-g-MA-rGO and PP-g-MA-rGOcyst.

Sample	ΔH_m / J g^{-1}	ΔH_c / J g^{-1}	T_m / °C	T_c / °C	X_c /%
PP-g-MA	83.66	80.15	α: 155.61 β: 148.43	110.27	35
PP-g-MA-rGO	67.56	58.92	α: 156.61 β: 148.43	118.64	23
PP-g-MA-rGOcyst	75.58	74.27	α: 157.12 β: 149.43	119.48	28

From the DSC thermograms shown in Figure 17 and the thermal parameters listed in Table , as PP-g-MA is heated, a double melting peak emerges at 148.4°C and 156.5°C, which is also seen for PP-g-MA-rGOcyst and PP-g-MA-rGO samples. The peak at lower temperature is attributed to the β-polymorph of PP, and the one at higher temperature the α-polymorph for PP [55]. Inclusion of rGO in both, PP-g-MA-rGO and PP-g-MA-rGOcyst, resulted in a decrease in X_c (also ΔH_c and ΔH_m). The interfacial interactions with the rGO hinders polymer chain dynamics and formation of regular crystalline structure and therefore contributes to increased amorphous fraction resulting in decreased enthalpies and crystalline content [56]. Furthermore, rGO acts as a β-nucleating agent, the intensity of the β-peak in increased relative to the α-peak. Furthermore, for composites of rGO or rGO-cyst and PP-g-MA the crystallization temperature (T_c) increased from 110°C to 119°C relative to unreacted PP-g-MA, behaviour associated with strong heterogeneous nucleation by the nano-filler for the polymer [57]. 2D nanomaterials are known to be efficient nucleating agents for polymers

increasing the rate of crystallization by introducing abundant nucleating sites [44]. Furthermore, due to the decrease in crystallinity (increase in the amorphous phase content), the crystallization peak becomes more broad. In the crystallization exotherm, only one peak is seen in spite of the formation of both α- and β-polymorphs as their formation occurs simultaneously when crystallized [58].

It is critical for industrial application that the cysteamine functionalised rGO is stable at the temperatures required for melt mixing with polymers. To this end, the thermal stability of cysteamine, rGO, rGO-cyst, PP-g-MA, PP-g-MA, PP-g-MA-rGO and PP-g-MA-rGOcyst was studied by TGA, Figure 18. Three main degradation pathways for GO can be highlighted, zones 1 through 3 (Z1, Z2 and Z3). Z1 corresponds to a 15% weight loss due to physically adsorbed water molecules within layers at < 50° C, Z2 correlates to a 30% weight loss and is associated with labile oxygen functional groups at ~210° C. Finally, in Z3 degradation a futher ~10% weight loss from the removal of more stable oxygen functionalities. Additionally, after cysteamine functionalisation, rGO-cyst exhibited similar thermal stability as rGO having only 27% weight loss over the temperature range studied. Furthermore, neat cysteamine starts to degrade at ~215°C in a one step process. For rGO-cyst there is a slight mass loss at that temperature relative to rGO. In the temperature range 215 to 350°C, rGO has a mass loss of ~1 wt%, whereas rGO-cyst has a mass loss ~5 wt%. This shows that the grafted cysteamine is present in rGO-cyst and it degrades during that temperature range. The thermal degradation of cysteamine is a one step-process with an onset temperature of ~ 220°C. From Figure 18 a), rGO has a weight loss of 11% between 100 and 800°C, whereas when grafted with cysteamine, this weight loss increased to 25% in the same temperature range. The degradation of PP-g-MA happens in one process with a peak at 364.5°C (Figure 18 b)) and is typical of that reported for the thermal degradation of PP [59]. However, the thermal degradation of PP-g-MA-rGOcyst was a two step process, with an

initial slightly lower onset at 200°C due to the degradation of cysteamine, but from ~400°C and above PP-g-MA-rGOcyst was more thermally stable than PP-g-MA-rGO and PP-g-MA, presumably due to the covalent bonding between cysteamine modified rGO an the maleic anhydride groups on PP-g-MA requiring higher energy to break bonds.

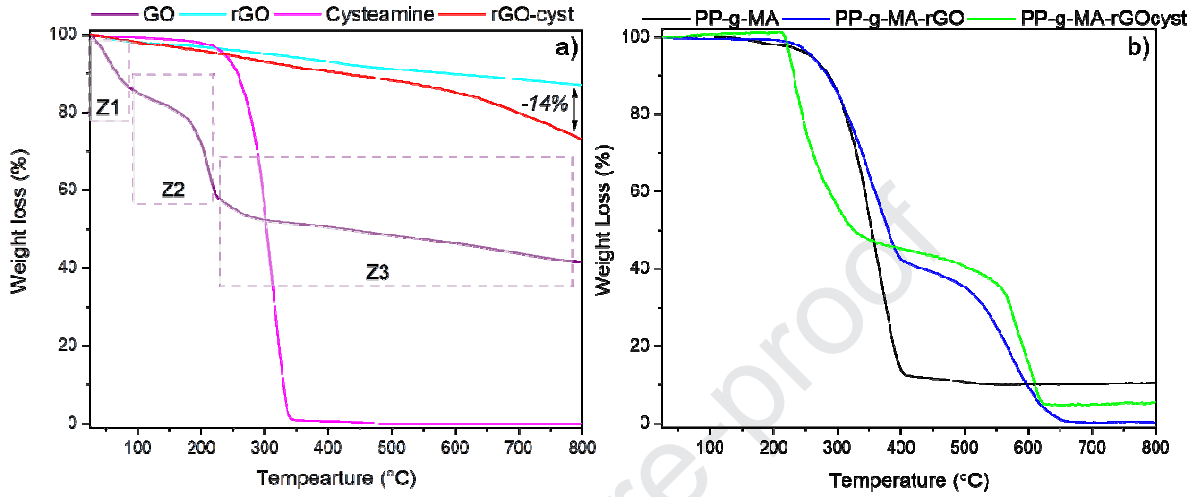

Figure 18. TGA curves (weight loss as a function of temperature) for a) cysteamine, GO, rGO, rGO-cyst and b) for PP-g-MA, PP-g-MA-rGO and PP-g-MA-rGOcyst.

4. Conclusions

GO was successfully reduced to rGO using hydrazine and ammonia as reducing agent. In removing oxygen functionalities, this reductant also introduced nitrogen functionalities by reacting with the carbonyls present on the basal plane of rGO. From NMR and XPS experiments, it was verified that pyrazolic structures were formed through reactions of hydrazine with diketones, creating amino groups on the surface of rGO for further reactions. Additionally, rGO-cyst was successfully functionalised using thiol-ene click chemistry. Detailed XPS analysis showed thiol reaction with both the double bonds of the rGO, and the pyrazolic structures, formed from the hydrazine treatment. This was confirmed by the evolution of a new peak at ~163 eV in the XPS showing the C-S bond and decreasing C=N to

C-N after cysteamine treatment. The amino group of the rGO-cyst was then further reacted with PP-g-MA to make PP-g-MA-rGOcyst. Through a combined ^{13}C MAS NMR, XPS and FTIR study, the reaction between the amine and the maleic anhydride was established and a mixture of open and closed ring structures proposed with amide, imine and imide functionalities. Comparison of SEM and TEM images of PP-g-MA-rGOcyst and PP-g-MA-rGO showed different polymer growth on the rGO surface. For PP-g-MA-rGOcyst growth appears to be associated with the polymer nucleating on the rGO surfaces and edges and therefore exfoliating the rGO layers, whereas, for PP-g-MA-rGO the growth of polymer was only on the rGO surface. From thermal studies PP-g-MA-rGOcyst was more crystalline than PP-g-MA-rGO and the T_c of PP-g-MA increased by 9°C on reaction with rGO-cyst. Inclusion of rGO nucleated PP-g-MA and induced the formation of the β-polymorphy of PP. PP-g-MA-rGOcyst was more thermally stable than PP-g-MA-rGO due to a covalent attachment between rGO and PP-g-MA *via* cysteamine bonding.

Acknowledgements

SA thanks EPSRC and Jaguar Land Rover for funding an iCASE PhD studentship. JVH acknowledges support for the solid state NMR instrumentation at Warwick used in this research which was funded by EPSRC (grant numbers EP/M028186/1 & EP/K024418/1) and the University of Warwick, with additional partial funding being provided through the Birmingham Science City Advanced Materials Projects 1 and 2, which were supported by Advantage West Midlands (AWM) and the European Regional Development Fund (ERDF). NLK thanks EPSRC for a PhD studentship through the EPSRC Centre for Doctoral Training in Molecular Analytical Science, grant number EP/L015307/1.

References

[1] H. Hu, G. Chen, Electrochemically modified graphite nanosheets and their nanocomposite films with poly(vinyl alcohol), Polym. Compos. 31(10) (2010) 1770-1775.

[2] A.A. Balandin, S. Ghosh, W. Bao, I. Calizo, D. Teweldebrhan, F. Miao, C.N. Lau, Superior Thermal Conductivity of Single-Layer Graphene, Nano Letters 8(3) (2008) 902-907.

[3] J. Zhang, Y. Xu, L. Cui, A. Fu, W. Yang, C. Barrow, J. Liu, Mechanical properties of graphene films enhanced by homo-telechelic functionalized polymer fillers via π–π stacking interactions, Composites Part A: Applied Science and Manufacturing 71 (2015) 1-8.

[4] H. Chen, M.B. Müller, K.J. Gilmore, G.G. Wallace, D. Li, Mechanically Strong, Electrically Conductive, and Biocompatible Graphene Paper, Advanced Materials 20(18) (2008) 3557-3561.

[5] N.G. Chopra, A. Zettl, Measurement of the elastic modulus of a multi-wall boron nitride nanotube, Solid State Communications 105(5) (1998) 297-300.

[6] R. Rohini, P. Katti, S. Bose, Tailoring the interface in graphene/thermoset polymer composites: A critical review, Polymer 70 (2015) A17-A34.

[7] R.R. Nair, P. Blake, A.N. Grigorenko, K.S. Novoselov, T.J. Booth, T. Stauber, N.M.R. Peres, A.K. Geim, Fine Structure Constant Defines Visual Transparency of Graphene, Science 320(5881) (2008) 1308-1308.

[8] L. Liao, H. Peng, Z. Liu, Chemistry Makes Graphene beyond Graphene, JACS 136(35) (2014) 12194-12200.

[9] A.K. Geim, K.S. Novoselov, The rise of graphene, Nat Mater 6(3) (2007) 183-191.

[10] D. Konios, M.M. Stylianakis, E. Stratakis, E. Kymakis, Dispersion behaviour of graphene oxide and reduced graphene oxide, Journal of Colloid and Interface Science 430 (2014) 108-112.

[11] H.R. Thomas, S.P. Day, W.E. Woodruff, C. Vallés, R.J. Young, I.A. Kinloch, G.W. Morley, J.V. Hanna, N.R. Wilson, J.P. Rourke, Deoxygenation of Graphene Oxide: Reduction or Cleaning?, Chemistry of Materials 25(18) (2013) 3580-3588.

[12] T.-H. Le, Y. Oh, H. Kim, H. Yoon, Exfoliation of 2D Materials for Energy and Environmental Applications, Chemistry – A European Journal 26(29) (2020) 6360-6401.

[13] H.J. Salavagione, Promising alternative routes for graphene production and functionalization, Journal of Materials Chemistry A 2(20) (2014) 7138-7146.

[14] M. Castelaín, G. Martínez, C. Marco, G. Ellis, H.J. Salavagione, Effect of Click-Chemistry Approaches for Graphene Modification on the Electrical, Thermal, and Mechanical Properties of Polyethylene/Graphene Nanocomposites, Macromol. 46(22) (2013) 8980-8987.

[15] Z. Peng, H. Li, Q. Li, Y. Hu, Microwave-Assisted thiol-ene click chemistry of carbon nanoforms, Colloids and Surfaces A: Physicochemical and Engineering Aspects 533 (2017) 48-54.

[16] B. Iskin, G. Yilmaz, Y. Yagci, Mono-addition Synthesis of Polystyrene–Fullerene (C60) Conjugates by Thiol–Ene Chemistry, Chemistry – A European Journal 18(33) (2012) 10254-10257.

[17] N.D. Luong, L.H. Sinh, L.-S. Johansson, J. Campell, J. Seppälä, Functional Graphene by Thiol-ene Click Chemistry, Chemistry – A European Journal 21(8) (2015) 3183-3186.

[18] D. Xu, M. Liu, Q. Huang, J. Chen, H. Huang, F. Deng, J. Tian, Y. Wen, X. Zhang, Y. Wei, A Novel method for the preparation of fluorescent C60 poly(amino acid) composites and their biological imaging, Journal of Colloid and Interface Science 516 (2018) 392-397.

[19] S. Vazquez-Rodriguez, S. Sánchez-Valdes, F.J. Rodríguez-González, M.C. González-Cantú, Influence of Low-Molecular-Weight Diamines in the Direct Imidation of

Poly(propylene)-Grafted Maleic Anhydride by Melt Reaction, Macromolecular Materials and Engineering 292(9) (2007) 1012-1019.

[20] J.G. Martínez-Colunga, S. Sanchez-Valdes, L.F. Ramos-deValle, O. Perez-Camacho, E. Ramirez-Vargas, R. Benavides-Cantú, C.A. Avila-Orta, V.J. Cruz-Delgado, J.M. Mata-Padilla, T. Lozano-Ramírez, A.B. Espinoza-Martínez, Aniline-Modified Polypropylene as a Compatibilizer in Polypropylene Carbon Nanotube Composites, Polymer-Plastics Technology and Engineering 57(13) (2018) 1360-1366.

[21] S.H. Jin, C.H. Kang, K.H. Yoon, D.S. Bang, Y.-B. Park, Effect of compatibilizer on morphology, thermal, and rheological properties of polypropylene/functionalized multi-walled carbon nanotubes composite, Journal of Applied Polymer Science 111(2) (2009) 1028-1033.

[22] K. Petrie, M. Kontopoulou, A. Docoslis, Noncovalent compatibilization of polypropylene/MWCNT composites using an amino-pyridine grafted polypropylene matrix, Polymer Composites 37(9) (2016) 2794-2802.

[23] M.-C. Hsiao, S.-H. Liao, Y.-F. Lin, C.-A. Wang, N.-W. Pu, H.-M. Tsai, C.-C.M. Ma, Preparation and characterization of polypropylene-graft-thermally reduced graphite oxide with an improved compatibility with polypropylene-based nanocomposite, Nanoscale 3(4) (2011) 1516-1522.

[24] Y. Cao, J. Feng, P. Wu, Polypropylene-grafted graphene oxide sheets as multifunctional compatibilizers for polyolefin-based polymer blends, Journal of Materials Chemistry 22(30) (2012) 14997-15005.

[25] Y. Lin, J. Jin, M. Song, Preparation and characterisation of covalent polymer functionalized graphene oxide, Journal of Materials Chemistry 21(10) (2011) 3455-3461.

[26] R.K. Harris, E.D. Becker, S.M. Cabral de Menezes, R. Goodfellow, P. Granger, NMR Nomenclature: Nuclear Spin Properties and Conventions for Chemical Shifts: IUPAC Recommendations 2001, Solid State Nuclear Magnetic Resonance 22(4) (2002) 458-483.

[27] J. Dechant, Polymer handbook. 3rd edition. J. BRANDRUP and E. H. IMMERGUT (editors). ISBN 0-471-81244-7. New York/Chichester/Brisbane/Toronto/Singapore: John Wiley & Sons 1989. Cloth bond, ca. 1850 pages, £ 115.00, $175.00, Acta Polymerica 41(6) (1990) 361-362.

[28] O.M. Musa, Handbook of Maleic Anhydride Based Materials, Springer2016.

[29] C.R. Kemnitz, M.J. Loewen, “Amide Resonance” Correlates with a Breadth of C−N Rotation Barriers, JACS 129(9) (2007) 2521-2528.

[30] S. Park, Y. Hu, J.O. Hwang, E.-S. Lee, L.B. Casabianca, W. Cai, J.R. Potts, H.-W. Ha, S. Chen, J. Oh, S.O. Kim, Y.-H. Kim, Y. Ishii, R.S. Ruoff, Chemical structures of hydrazine-treated graphene oxide and generation of aromatic nitrogen doping, Nature Communications 3(1) (2012) 638.

[31] J.A. Joule, K. Mills, Heterocyclic Chemistry, John Wiley & Sons2010.

[32] S. Stankovich, D.A. Dikin, R.D. Piner, K.A. Kohlhaas, A. Kleinhammes, Y. Jia, Y. Wu, S.T. Nguyen, R.S. Ruoff, Synthesis of graphene-based nanosheets via chemical reduction of exfoliated graphite oxide, Carbon 45(7) (2007) 1558-1565.

[33] S. Park, R.S. Ruoff, Chemical methods for the production of graphenes, Nature Nanotechnology 4(4) (2009) 217-224.

[34] A.N. Koreshkova, V. Gupta, A. Peristyy, P.N. Nesterenko, T. Rodemann, B. Paull, Ion chromatographic determination of hydrazine in excess ammonia for monitoring graphene oxide reduction reaction, Talanta 205 (2019) 120081.

[35] S.S. Abbas, G.J. Rees, N.L. Kelly, C.E.J. Dancer, J.V. Hanna, T. McNally, Facile silane functionalization of graphene oxide, Nanoscale 10(34) (2018) 16231-16242.

[36] W. Cai, R.D. Piner, F.J. Stadermann, S. Park, M.A. Shaibat, Y. Ishii, D. Yang, A. Velamakanni, S.J. An, M. Stoller, J. An, D. Chen, R.S. Ruoff, Synthesis and Solid-State NMR Structural Characterization of ¹³C-Labeled Graphite Oxide, Science 321(5897) (2008) 1815-1817.

[37] A. Buchsteiner, A. Lerf, J. Pieper, Water Dynamics in Graphite Oxide Investigated with Neutron Scattering, The Journal of Physical Chemistry B 110(45) (2006) 22328-22338.

[38] T. Axenrod, P.S. Pregosin, M.J. Wieder, E.D. Becker, R.B. Bradley, G.W.A. Milne, Nitrogen-15 nuclear magnetic resonance spectroscopy. Substituent effects on 15N-H coupling constants and nitrogen chemical shifts in aniline derivatives, Journal of the American Chemical Society 93(24) (1971) 6536-6541.

[39] T. Nakaoki, Y. Inaji, Molecular Structure of Isotactic Polypropylene Formed from Homogeneous Solution. Gelation and Crystallization, Polymer Journal 34(7) (2002) 539-543.

[40] R. Zhang, Y. Zhu, J. Zhang, W. Jiang, J. Yin, Effect of the initial maleic anhydride content on the grafting of maleic anhydride onto isotactic polypropylene, Journal of Polymer Science Part A: Polymer Chemistry 43(22) (2005) 5529-5534.

[41] C.-C. Bi, X.-X. Ke, X. Chen, R. Weerasooriya, Z.-Y. Hong, L.-C. Wang, Y.-C. Wu, Assembling reduced graphene oxide with sulfur/nitrogen- “hooks” for electrochemical determination of Hg(II), Analytica Chimica Acta 1100 (2020) 31-39.

[42] T.B. Albuquerque, C.D.G. da Silva, A.R. de Oliveira, B.F. dos Santos, B.A.L. da Silva, R. Katla, M.P.D. Rocha, N.L.C. Domingues, Lipase catalyzed 1,2-addition of thiols to imines under mild conditions, New Journal of Chemistry 42(3) (2018) 1642-1645.

[43] P.L. Yap, S. Kabiri, Y.L. Auyoong, D.N.H. Tran, D. Losic, Tuning the Multifunctional Surface Chemistry of Reduced Graphene Oxide via Combined Elemental Doping and Chemical Modifications, ACS Omega 4(22) (2019) 19787-19798.

[44] G. George, S.M. Simon, P. V. P, S. M. S, M. Faisal, R. Wilson, A. Chandran, B. P. R, C. Joseph, N.V. Unnikrishnan, Green and facile approach to prepare polypropylene/in situ reduced graphene oxide nanocomposites with excellent electromagnetic interference shielding properties, RSC Adv. 8(53) (2018) 30412-30428.

[45] S.-H. Hsiao, Y.-T. Chiu, Synthesis and characterization of novel electrochromic poly(amide-imide)s with N,N'-di(4-methoxyphenyl)-N,N'-diphenyl-p-phenylenediamine units, RSC Adv. 5 (2015).

[46] S. Kabiri, D.N.H. Tran, M.A. Cole, D. Losic, Functionalized three-dimensional (3D) graphene composite for high efficiency removal of mercury, Environmental Science: Water Research & Technology 2(2) (2016) 390-402.

[47] S. Kabiri, D.N.H. Tran, S. Azari, D. Losic, Graphene-Diatom Silica Aerogels for Efficient Removal of Mercury Ions from Water, ACS Appl. Mater. Inter. 7(22) (2015) 11815-11823.

[48] P.L. Yap, S. Kabiri, D.N.H. Tran, D. Losic, Multifunctional Binding Chemistry on Modified Graphene Composite for Selective and Highly Efficient Adsorption of Mercury, ACS Applied Materials & Interfaces 11(6) (2019) 6350-6362.

[49] A.M. Rao, P.C. Eklund, S. Bandow, A. Thess, R.E. Smalley, Evidence for charge transfer in doped carbon nanotube bundles from Raman scattering, Nature 388(6639) (1997) 257-259.

[50] S.H. Ryu, A.M. Shanmugharaj, Influence of long-chain alkylamine-modified graphene oxide on the crystallization, mechanical and electrical properties of isotactic polypropylene nanocomposites, Chemical Engineering Journal 244 (2014) 552-560.

[51] X. Duan, K. O'Donnell, H. Sun, Y. Wang, S. Wang, Sulfur and Nitrogen Co-Doped Graphene for Metal-Free Catalytic Oxidation Reactions, Small 11(25) (2015) 3036-3044.

[52] M.-C. Hsiao, S.-H. Liao, M.-Y. Yen, P.-I. Liu, N.-W. Pu, C.-A. Wang, C.-C.M. Ma, Preparation of Covalently Functionalized Graphene Using Residual Oxygen-Containing Functional Groups, ACS Applied Materials & Interfaces 2(11) (2010) 3092-3099.

[53] H. Xia, Q. Wang, K. Li, G.-H. Hu, Preparation of polypropylene/carbon nanotube composite powder with a solid-state mechanochemical pulverization process, Journal of Applied Polymer Science 93(1) (2004) 378-386.

[54] M. Liu, B. Guo, M. Du, F. Chen, D. Jia, Halloysite nanotubes as a novel β-nucleating agent for isotactic polypropylene, Polymer 50(13) (2009) 3022-3030.

[55] J. Dai, X.-h. Liu, J.-h. Yang, N. Zhang, T. Huang, Y. Wang, Z.-w. Zhou, Stretching induces pore formation in the β-nucleated polypropylene/graphene oxide composite, Composites Science and Technology 99 (2014) 59-66.

[56] A. Bhattacharyya, S. Chen, M. Zhu, Graphene reinforced ultra high molecular weight polyethylene with improved tensile strength and creep resistance properties, Express Polymer Letters 8(2) (2014).

[57] S. Zhao, F. Chen, C. Zhao, Y. Huang, J.-Y. Dong, C.C. Han, Interpenetrating network formation in isotactic polypropylene/graphene composites, Polymer 54(14) (2013) 3680-3690.

[58] R. Krache, R. Benavente, J.M. López-Majada, J.M. Pereña, M.L. Cerrada, E. Pérez, Competition between α, β, and γ Polymorphs in a β-Nucleated Metallocenic Isotactic Polypropylene, Macromolecules 40(19) (2007) 6871-6878.

[59] A. Fina, D. Tabuani, T. Peijs, G. Camino, POSS grafting on PPgMA by one-step reactive blending, Polymer 50(1) (2009) 218-226.

Highlights

- Cysteamine functionalised rGO reacted with PP-g-MA
- Reaction confirmed from MAS NMR, FTIR and XPS studies
- Cysteamine acts like a ‘cross-linker’ between rGO and PP-g-MA
- Crystallisation behaviour of PP-g-MA altered on reaction with rGO-cyst

Declaration of interests

☒ The authors declare that they have no known competing financial interests or personal relationships that could have appeared to influence the work reported in this paper.

☐The authors declare the following financial interests/personal relationships which may be considered as potential competing interests: